A *Drosophila* model of Huntington disease-like 2 exhibits nuclear toxicity and distinct pathogenic mechanisms from Huntington disease

Megan Krench[1], Richard Cho[1,2], and J. Troy Littleton[1,2,*]

[1]The Picower Institute for Learning and Memory and Department of Brain and Cognitive Sciences, [2]Department of Biology, Massachusetts Institute of Technology, Cambridge, MA 02139, USA

[*]Corresponding author:

J. Troy Littleton

43 Vassar St, 46-3243, Cambridge, MA 02139

Fax: 617-452-2249

Phone: 617-452-2605

Email: troy@mit.edu

Abstract

Huntington disease-like 2 (HDL2) and Huntington disease (HD) are adult-onset neurodegenerative diseases characterized by movement disorders, psychiatric disturbances and cognitive decline. Brain tissue from HD and HDL2 patients show degeneration of the striatum and ubiquitinated inclusions immunoreactive for polyglutamine (polyQ) antibodies. Despite these similarities, the diseases result from different genetic mutations. HD is caused by a CAG repeat expansion in the *huntingtin* (*HTT*) gene, while HDL2 results from expansion at the *junctophilin 3* locus. Recent evidence indicates the HDL2 expansion may give rise to a toxic polyQ protein transcribed from an antisense mRNA derived from the *junctophilin* locus. To investigate this hypothesis, we generated and characterized a *Drosophila* HDL2 model and compared it to a previously established HD model. We find that neuronal expression of HDL2-Q15 is not toxic, while expression of an expanded HDL2-Q138 protein is lethal. HDL2-Q138 forms large nuclear aggregates, with only smaller puncta observed in the cytoplasm. This is in contrast to what is observed in a *Drosophila* model of HD, where polyQ aggregates localize exclusively to the cytoplasm. Altering localization of HLD2 with the addition of a nuclear localization or nuclear export sequence demonstrates nuclear accumulation is required for toxicity in the *Drosophila* HDL2 model. Directing HDL2-Q138 to the nucleus exacerbates toxicity in multiple tissue types, while confining HDL2-Q138 to the cytoplasm restores viability to control levels. We conclude that while HD and HDL2 have similar clinical profiles, distinct pathogenic mechanisms are likely to drive toxicity in *Drosophila* models of these disorders.

Introduction

Huntington disease like 2 (HDL2) is an autosomal dominant neurodegenerative disorder with symptoms and neuropathology strikingly similar to Huntington disease (HD) (1). Symptoms include chorea, psychiatric disturbances and cognitive decline with death resulting approximately 15 years after onset (2). Patients' brains show extensive degeneration of the caudate nucleus and cortical thinning (2). Ubiquitinated intranuclear inclusions that stain with 1C2, an antibody that detects polyglutamine (polyQ) proteins, are a hallmark of the disorder (2). In spite of symptomatic and neuropathological similarities to HD, HDL2 patients do not have a mutation in the *huntingtin* (*HTT*) gene. The HDL2 mutation results from a CTG/CAG trinucleotide repeat expansion at the *junctophilin 3* locus on chromosome 16 (3). As with HD, the number of tandem repeats varies among healthy individuals; in both HD and HDL2, the disease state results from expansions greater than approximately 40 repeats. Depending on the frame, the mutation in HDL2 could result in a polyleucine expansion, a polyalanine expansion, or an expansion in the 3' UTR (3). However, expanded polyalanine or polyleucine proteins have not been detected in HDL2 patient brain samples (4).

Several mechanisms of toxicity have been proposed to contribute to HDL2 pathogenesis. First, the expansion may impair transcription of *JPH3*, leading to a loss of function (4). Another potential pathogenic pathway is RNA toxicity from expanded CUG transcripts. Expanded CUG transcripts have been shown to cause toxicity in several diseases, including Machado-Joseph disease (MJD), spinocerebellar ataxia 8 (SCA8), and myotonic dystrophy 1 (DM1) (5–7). CUG RNA foci have been found in postmortem HDL2 patient brain tissue, and staining indicates the RNA splicing protein muscleblind is sequestered in these foci (8). While CUG RNA toxicity may contribute to HDL2 pathogenesis, it does not explain the existence of ubiquitinated aggregates in patients' brains. Protein aggregates and RNA foci rarely, if ever, co-localize (2),

suggesting protein aggregates may be the result of a separate pathogenic pathway.

Recently, toxicity in microsatellite expansion diseases has been suggested to occur from transcripts originating in both sense and antisense directions. Pathology resulting from bidirectional transcription has been described in several CTG expansion diseases, including SCA8, HDL2 (9–11), and others (11). Antisense transcription across the CTG expansion in *JPH3* results in an expanded CAG transcript, which, if translated, produces a novel polyQ protein. Several lines of evidence support a polyQ pathology model in HDL2. First, the presence of an active promoter on the antisense strand is supported by bioinformatics and confirmed experimentally using luciferase reporter assays (4, 10). Bidirectional transcription across the *JPH3* locus has also been demonstrated by the presence of expanded CAG transcripts in a BAC HDL2 mouse model (10). Experiments in postmortem human tissue reveal the presence of an antisense CAG transcript (4). Importantly, in HDL2 patient brain tissue, immunohistochemistry has demonstrated 1C2-positive intranuclear inclusions in HDL2 patients' motor cortex and amygdala (2). Evidence of polyQ protein production has also been found in the HDL2 mouse model using the polyQ antibodies 1C2 and 3B5H10 (10). Further support for the role of an antisense transcript comes from sequencing the sense and antisense transcriptomes of human cells (12). Of the 10,000 genes analyzed, most demonstrated transcription primarily in the sense orientation, while a small subset demonstrated significant transcriptional activity in both directions. Fewer than 2.5% of genes were classified as primarily antisense. Transcription at *JPH3* falls into the last, rare category.

To investigate how an HDL2 polyQ protein may exert toxicity, we generated transgenic *Drosophila* harboring the human antisense *HDL2-CAG* transcript. We compared mechanisms of toxicity to those observed in a Huntington Disease *Drosophila* model we previously generated,

or in *Drosophila* expressing a pure polyQ tract. Despite the similar neuropathology between HD and HDL2 patients, we observe that the polyQ proteins promote toxicity through localization in different subcellular compartments in *Drosophila* neurons. The HDL2 polyQ protein is also distinct from a pure polyQ tract, indicating that protein context is critical to polyQ disease pathology. Finally, we find that nuclear localization of the expanded polyQ HLD2 protein is required for toxicity, in contrast to the purely cytoplasmic localization of toxic polyQ HTT proteins in the *Drosophila* models.

Results

Generating *Drosophila* models of HDL2

CAG transcripts from the antisense strand of *JPH3* have been found in both BAC HDL2 model mice and post-mortem human brain tissue (4, 10). 5' RACE experiments in the BAC HDL2 mouse model indicate two active start sites (10). The full-length isoform was selected for our experiments (Seixas *et al.*, 2012; Wilburn *et al.*, 2011). The protein encoded by this transcript is 82 amino acids, plus the length of the polyQ region. A schematic of the *JPH3* locus, antisense open reading frame, and sequence in shown in Figure 1A and B. No HGNC-approved gene symbols have been determined for the antisense *CAG* product. We refer to the antisense gene at the *JPH3* locus that contributes to toxicity in HDL2 as *HDL2*, and the polyQ protein product as HDL2. *De novo* synthesis of the antisense transcripts with either 15 or 138 CAG repeats was performed. These constructs are referred to as *HDL2-Q15* and *HDL2-Q138*. *HDL2-Q15* is 291 base pairs (97 amino acids, 11 kDa), and *HDL2-Q138* is 660 base pairs (220 amino acids, 27 kDa). Although repeat lengths larger than 60 have not yet been observed in HDL2, we choose a larger Q138 repeat length to be able to compare phenotypes to a previously generated HD Q138 model we have generated.

Before generating *Drosophila* models, we tested these constructs in insect S2 cell cultures. Transfection in S2 cells revealed that the expanded GFP-HDL2-Q138 proteins form large aggregates, while GFP-HDL2-Q15 remains diffuse or forms smaller aggregates (Supplementary Material, Figs. S1A, S1B). HDL2 protein distribution in S2 cells is similar to that of expanded mRFP-HTT-Q138 (aggregated) or non-pathogenic RFP-HTT-Q15 (diffuse) (Supplementary Material, Fig. S1C). *HDL2-Q15* and *–Q138* constructs were subsequently cloned into *Drosophila* expression vectors for integration into the embryonic germline. Three

variants were made for each gene: untagged, N-terminal GFP tag and N-terminal mRFP tag (Fig. 1C). The constructs were inserted at random sites in the *Drosophila* genome to allow for transgenic lines expressing varying levels of the HDL2 protein. The resulting flies carry an upstream activating sequence (*UAS*) in front of *HDL2-Q15* or *–Q138*, allowing for temporal and spatial control via the *UAS-GAL4* system. Given that HDL2 and HD patients share similar neuropathologies, we investigated whether mechanisms of toxicity might be similar between the two proteins in *Drosophila* models. We selected HD model flies that we previously generated using a caspase-6 cleavage fragment of the human *HTT* gene downstream of a *UAS* sequence. The resulting protein is comprised of the first 588 amino acids of HTT, contains 138 CAG repeats, and can be visualized by its N-terminal mRFP tag (13). To ensure the effects of HDL2-Q138 expression are the result of the unique protein context and not simply due to the polyQ tract, we also compared HDL2 transgenic flies to those expressing a pure polyQ protein, Q127 (14). The *Q127* transgene is downstream of a *UAS* sequence and tagged with HA.

Neuronal expression of HDL2-Q138 causes dose-dependent lethality

To investigate the effects of HDL2 expression in *Drosophila*, *UAS-HDL2* flies were crossed to *elav-GAL4* flies to generate progeny that expressed *HDL2* transgenes strongly throughout the nervous system. Pan-neuronal expression of *HDL2-Q15* is not toxic in any of the lines we generated. There was no difference between animals expressing untagged, GFP-tagged, and mRFP-tagged constructs. Conversely, pan-neuronal expression of *HDL2-Q138* was highly toxic. Due to random genomic integration of the construct, *UAS-HDL2* lines have varying expression levels as observed by fluorescent intensity of the expressed tagged HDL2 proteins. In strong expressing lines, *elav>HDL2-Q138* resulted in early pupal lethality, with animals dying

shortly after the 3rd instar larval stage. There was no difference in toxicity between flies expressing untagged HDL2-Q138 versus constructs with mRFP or GFP tags. An mRFP-tagged, high expression line was selected for use in the rest of the experiments. As observed for HDL2-Q138, pan-neuronal expression of mRFP-HTT-Q138 or Q127-HA is also lethal before adulthood.

HDL2-Q15 is soluble, while HDL2-Q138 aggregates localize to different compartments across specific cell types

To determine the subcellular compartment potentially responsible for HDL2 toxicity, we analyzed the localization of mRFP-HDL2-Q15 and mRFP-HDL2-Q138 in three cell types: multidendritic peripheral neurons (*pickpocket-GAL4*), muscle cells (*mef2-GAL4*) and epithelial cells of the salivary gland (*elav-GAL*, a neuronal driver that also expresses in salivary glands). In all cell types tested, mRFP-HDL2-Q15 remained diffuse throughout the nucleus and cytoplasm, occasionally forming small puncta (Figs. 2A, E, I). In contrast, mRFP-HDL2-Q138 aggregated in all cell types tested, with inclusions forming in distinct compartments across different tissues (Figs. 2B, F, J). In multidendritic peripheral neurons, mRFP-HDL2-Q138 aggregates in the nucleus (Fig. 2B). mRFP-HDL2-Q138 localization in muscles is similar to that observed in neurons: nuclear aggregates are always observed, and the protein appears as smaller puncta in the cytoplasm (Fig. 2F). In contrast to nuclear aggregates formed in neurons and muscles, strong expression of mRFP-HDL2-Q138 in salivary gland epithelial cells leads to cytoplasmic aggregates (Fig. 2J). Hence, aggregates are consistently observed in all tissues examined, but the distribution of mRFP-HDL2-Q138 varies in different cell types.

We next compared the localization of mRFP-HDL2-Q138 to that of mRFP-HTT-Q138.

While mRFP-HDL2-Q138 forms nuclear aggregates in neurons and muscles, mRFP-HTT-Q138 is strictly cytoplasmic in these tissues in the *Drosophila* HD model. mRFP-HTT-Q138 is not observed in the nucleus of neurons, muscles, or epithelial cells (Figs. 2C, G, K). In HD patients and mammalian models, N terminal fragments produced by caspase and calpain cleavage events have been found to cause nuclear aggregates (15–18). *Drosophila* do not cleave HTT to liberate smaller N terminal pieces from the 588-amino acid fragment expressed in our model, which may explain why the protein remains confined to the cytoplasm (13).

We next compared mRFP-HDL2-Q138 localization to that of Q127-HA, a pure polyQ tract with no surrounding protein. As with mRFP-HDL2-Q138, neuronal expression of Q127-HA leads to nuclear aggregates in neurons (Fig. 2D). Similarly, Q127-HA aggregates in the nuclei of muscle cells (Fig. 2H). Q127-HA puncta are rarely observed in the muscle cytoplasm. A pronounced distinction between mRFP-HDL2-Q138 and Q127-HA localization was observed in salivary gland epithelial cells. While mRFP-HDL2-Q138 aggregates in the cytoplasm of this cell type, Q127-HA forms nuclear aggregates (Figs. 2J, L). These experiments indicate HDL2 aggregation is polyQ-length dependent in both neuronal and non-neuronal cell types. Furthermore, mRFP-HDL2-Q138 localization is distinct from that of pathogenic mRFP-HTT-Q138 or a pure polyQ tract. Table 1 summarizes the localization of mRFP-HDL2-Q138, mRFP-HTT-Q138, and Q127-HA in the cell types analyzed.

HDL2-Q138 expression does not induce axonal trafficking or synaptic defects

We next investigated and compared mRFP-HDL2-Q138 and mRFP-HttQ138 expression in glutamatergic motor neurons and neuromuscular junction (NMJ) synapses using *elav-GAL4*. As previously observed, mRFP-HTT-Q138 forms large immobile aggregates along axons (Fig.

3E) that interfere with axonal transport and result in the accumulation of transport cargo at these sites of blockage (13). As observed in peripheral neurons, mRFP-HDL2-Q138 expression results in aggregates in the nucleus of ventral nerve cord (VNC) motor neurons (Fig. 3A). mRFP-HDL2-Q138 often forms a single nuclear inclusion, but low levels of soluble mRFP-HDL2-Q138 are also observed in nuclei. The HDL2-Q138 protein is also trafficked along axons as small aggregates or puncta (Fig. 3D), but does not lead to large axonal aggregates or a blockage in axonal transport as observed with pathogenic HTT. In contrast to HDL2 and HTT pathogenic proteins, we did not observe Q127-HA in axons, but instead found it in nuclear aggregates (Figs. 3C, F). We conclude that HDL2 does not manifest large axonal aggregates that disrupt transport as observed in our *Drosophila* HD model (13).

We next examined NMJ synaptic terminals where motor neurons contact muscle fibers. After contacting the muscle fiber, immature filopodia at the NMJ develop synaptic varicosities, termed boutons, which serve as site for communication between nerve and muscle (19). The relationship between the neuron and muscle is plastic and changes in response to neural activity and muscle growth. Failure to coordinate activity-dependent synaptic growth can lead to under- or over-developed NMJs. Both soluble and aggregated mRFP-HTT-Q138 readily localize to the synapse, and expression of mRFP-HTT-Q138 induces synaptic overgrowth with supernumerary satellite boutons due to a disruption in the trafficking of synaptic growth factor receptors (Fig. 3H, Akbergenova and Littleton, unpublished data). Small mRFP-HDL2-Q138 puncta are occasionally found at synaptic boutons, but the toxic protein does not form large aggregates like those observed in nuclei, and does not induce synaptic overgrowth (Fig. 3G, arrowheads). As such, the peripheral pathologies associated with pathogenic HTT on axonal transport and synaptic development are absent in the HDL2 model. To look for more subtle defects in synaptic

properties, we performed electrophysiology at the NMJ to determine if mHDL2-Q138 perturbed synaptic transmission. Neuronal expression of mRFP-HDL2-Q138 did not significantly impair spontaneous or evoked release (Supplementary Material, Fig. S2), suggesting synaptic transmission is not disrupted at this stage of development by pathogenic HDL2. In contrast to HDL2 and Htt, the polyQ protein Q127-HA alone is not observed in axons or at the NMJ (Fig. 3F, I). Expression of Q127-HA also does not induce synaptic overgrowth (Fig. 3I), suggesting this effect is specific for the pathogenic HTT protein, which displays prominent synaptic aggregates.

mRFP-HDL2-Q138 does not localize to the nucleolus or impair nuclear import

Given the lack of axonal transport or synaptic transmission defects in HDL2 expressing animals, we examined other cellular compartments where toxicity could arise. Unlike mRFP-HTT-Q138, which remains in the cytoplasm, mRFP-HDL2-Q138 aggregates in neuronal nuclei. Within the nucleus, mRFP-HDL2-Q138 usually forms a single, dense aggregate. We hypothesized that mRFP-HDL2-Q138 may be aggregating within the nucleolus, which would suggest certain pathologies. The nucleolus is a non-membrane-bound subdomain within the nucleus where ribosomal subunits are assembled. In addition to its primary role in ribosome biogenesis, the nucleolus also plays roles in cellular stress responses, DNA damage and repair, and other processes (20). Nucleoli can be visualized by staining for fibrillarin, a component of rRNA processing machinery (21). As in wild-type animals, staining with anti-fibrillarin in *elav>mRFP-HDL2-Q138* larvae revealed a single nucleolus in each nucleus. mRFP-HDL2-Q138 aggregates did not co-localize with the nucleolus, nor did aggregates consistently appear adjacent to the nucleolus. These data indicate HDL2-Q138 aggregates and the nucleolus reside in separate

domains within the nucleus (Supplementary Material, Fig. S3).

We next investigated whether mRFP-HDL2-Q138 interrupts nuclear transport, a process recently shown to be defective in frontotemporal dementia and amyotrophic lateral sclerosis 1 (FTDALS1) models (22–24). Neuronal cell bodies are tightly packed in the brain, making it challenging to target just one nucleus for analysis. Therefore, we expressed mRFP-HDL2-Q138 or mRFP-HDL2-Q15 in muscle cells and analyzed nuclear import with fluorescence recovery after photobleaching (FRAP) experiments. *Drosophila* larval muscle fibers are large, multi-nucleate cells that are very accessible to FRAP. Using the *mef2-GAL4* muscle driver, we co-expressed mRFP-HDL2-Q15 or mRFP-HDL2–Q138 and a genetically encoded fluorescent protein fused to a nuclear localization signal (NLS), GPF-NLS. GFP-NLS is concentrated in the nuclei of muscle cells. If pathogenic HDL2 interfered with nuclear import, we hypothesized that nuclear GFP would recover more slowly in larvae expressing mRFP-HDL2-Q138 as compared to mRFP-HDL2-Q15. However, FRAP experiments did not reveal any difference in fluorescence recovery time between these genotypes (Supplementary Material, Fig. S4). These results suggest that disruption of nuclear import is not likely to be a primary pathogenic mechanism in this HDL2 model.

Addition of a nuclear import or nuclear export tag alters localization of HDL2

Given that soluble and aggregated mRFP-HDL2-Q138 localize to the nuclei of neurons, we examined if localization played a role in toxicity. Nuclear localization has been shown to be critical for disease pathogenesis in HD, spinocerebellar ataxia 1 (SCA1) and other polyQ disorders. One strategy would be to modify intrinsic NLS or nuclear export sequences (NES), but we could not identify any canonical NLS or NES within the HDL2 protein using bioinformatics

approaches. To redirect HDL2, we created transgenic *Drosophila* expressing HDL2 where we added a NLS or NES tag to the C terminus of HDL2-Q15 and HDL2-Q138, along with a GFP tag at the N terminus. Constructs expressing *GFP-HDL2-Q15* and *GFP-HDL2-Q138* with an NLS, NES, or no tag were inserted into the same *attP2* genetic docking site using the phiC31 targeted integration system, which ensures equal expression among all transgenic lines using the UAS system (Figs. 4A, D, G). Semi-quantitative RT-PCR of HLD2 confirmed that the lines express similar mRNA levels (Supplementary Material, Fig. S5). Lines obtained from these site-directed injections do not express transgenes as strongly as some of the lines obtained by integration at random sites. Hence, dose-dependent metrics like lethality differed from the mRFP-HDL2-Q138 high expression lines used in the previously described experiments. These site-directed lines will be denoted with superscript "attP2" to differentiate them from the random insertion lines described above.

First, we assayed if NLS and NES tags successfully redirected the HLD2 protein. We examined several tissue types, including the large, multinucleate larval muscle cells. Using the muscle driver *mef2-GAL4,* expression of GFP-HDL2-Q138^{attP2} results in large nuclear aggregates, along with small aggregates in the cytoplasm (Fig. 4B). Expression of GFP-HDL2-Q138-NLS^{attP2} also leads to nuclear aggregate formation, but lacks any detectable cytoplasmic HDL2-Q138 protein (Fig. 4E). In contrast, no nuclear fluorescence is observed in animals expressing GFP-HDL2-Q138-NES^{attP2}, and the protein is visible as only cytoplasmic aggregates (Fig. 4H). These experiments demonstrate that the NLS and NES tags redirect the HDL2 protein as intended.

Nuclear localization and polyQ tract expansion are required for HDL2 toxicity in muscles

After determining that the NLS and NES tags target the protein to the desired compartments, we investigated the effects of nuclear or cytoplasmic localization on toxicity. Using the *mef2-GAL4* muscle driver, expression of GFP-HDL2-Q138^{attP2} is lethal at the 3rd instar larval stage (Fig. 4C). Dead larvae appear dark colored, suggesting necrotic cell death is occurring. Toxicity is exacerbated with nuclear localization. Animals expressing GFP-HDL2-Q138-NLS^{attP2} die earlier in development, during the 2nd instar, and also turn a dark color (Fig. 4F). Strikingly, nuclear export completely rescues lethality, as animals with muscle expression of GFP-HDL2-Q138-NES^{attP2} are viable (Fig. 4I). Adult flies appear healthy, with no phenotypic abnormalities such as wing inflation defects or motor incoordination detected. We also expressed non-pathogenic GFP-HDL2-Q15^{attP2} in muscle. Muscle expression of all Q15 variants (GFP-HDL2-Q15^{attP2}, GFP-HDL2-Q15-NLS^{attP2}, and GFP-HDL2-Q15-NES^{attP2}) were adult viable. Hence, nuclear localization alone is not sufficient for toxicity. Instead, HDL2 toxicity requires both nuclear localization and the expanded polyQ tract.

Nuclear localization of HDL2-Q138 is required for neuronal toxicity

We next expressed GFP-HDL2-Q138^{attP2}, GFP-HDL2-Q138-NLS^{attP2} and GFP-HDL2-Q138-NES^{attP2} in the *Drosophila* eye using the GMR-GAL4 driver. The eye is comprised of hundreds of ommitidia, each containing eight photoreceptor neurons (Fig. 5A). This highly organized structure provides a conducive system to study neurodegenerative processes (25). Expression of GFP-HDL2-Q138^{attP2} does not result in any obvious defects in eye anatomy (Fig. 5B). GFP-HDL2-Q138-NES^{attP2} expression is also indistinguishable from controls (Fig. 5D). However, directing the HDL2 polyQ protein to the nucleus (GFP-HDL2-Q138-NLS^{attP2}) causes a severe rough eye degenerative phenotype, indicating that nuclear localization of expanded HDL2

enhances toxicity (Fig. 5C).

To examine how nuclear localization or export affects toxicity of the HDL2 protein in the CNS, we used *elav-GAL4* to express GFP-HDL2-Q138^{attP2}, GFP-HDL2-Q138-NLS^{attP2} or GFP-HDL2-Q138-NES^{attP2} throughout the nervous system. Neuronal expression of all three lines is adult viable due to the lower expression of genes from the *attP2* site. However, within days of eclosion, motor defects begin to appear. To measure motor deficits we employed a climbing assay, which quantified the percentage of flies that were able to climb two centimeters or more in a 30-second time period (Fig. 6A, Movie S1). Healthy flies exhibit negative geotaxis, immediately climbing upward when shaken to the bottom of a vial. One day after eclosion, flies expressing GFP-HDL2-Q138-NLS^{attP2} exhibit normal climbing behavior. However, one week after eclosion, flies with HDL2-NLS exhibit severely impaired motor function. Flies expressing the unmodified or NES constructs had no impairments at one week of age. By three weeks of age, GFP-HDL2-Q138^{attP2} flies failed to climb, while GFP-HDL2-Q138-NES ^{attP2} flies performed as well as controls. By week five, the climbing ability of HDL2-Q138-NES^{attP2} flies remained indistinguishable from controls. Hence, nuclear localization of GFP-HDL2-Q138 accelerates the onset of motor dysfunction, while nuclear export completely suppresses motor defects caused by GFP-HDL2-Q138 expression in the climbing assay.

Nuclear localization or nuclear export of HDL2-Q138 has an equally robust effect on lifespan (Fig. 6B). At 29°C, the median survival of control flies is 43 days. When GFP-HDL2-Q138^{attP2} is expressed in neurons with the *elav-GAL4* driver, median survival drops to 28 days. Nuclear localization further reduces lifespan, with GFP-HDL2-Q138-NLS^{attP2} flies displaying a median survival of 10 days. In contrast, nuclear export of HDL2 completely rescues the lifespan reduction. The median survival for flies expressing GFP-HDL2-Q138-NES^{attP2} is 45 days,

similar to controls. In conclusion, nuclear localization of HDL2-Q138 enhances toxicity in multiple tissue types (muscles, eyes, and neurons), while removal of HDL2-Q138 from the nucleus completely suppresses toxicity.

Discussion

We have generated and characterized a *Drosophila* HDL2 model to examine how an HDL2 polyQ protein may exert toxicity. In addition, we compared pathology to that we previously identified in one *Drosophila* HD model or strains that express a pure polyQ tract. Our findings indicate that nuclear localization of HLD2-Q138 is required for toxicity and that the HDL2 and HTT polyQ proteins cause toxicity in different cellular compartments in *Drosophila*.

In the current study, we found that expanded HDL2-Q15 is not toxic to *Drosophila*. HDL2-Q15 protein remains diffuse throughout the nucleus and the cytoplasm in cultured S2 cells, neurons, epithelial cells and muscles (Figs. 2A, E, I). Concentrating it in the nucleus with an NLS tag does not cause toxicity, suggesting the HDL2 unexpanded protein is nonpathogenic. While unmodified (HDL2-Q138^{attP2}) and nuclear-targeted (HDL2-Q138-NLS^{attP2}) versions of expanded HDL2 are pathogenic in muscle tissue, all HDL2-Q15^{attP2} constructs are viable to adulthood. Similarly, no defects are observed with neuronal expression of unmodified or NLS tagged HDL2-Q15^{attP2}. Hence, the combination of nuclear localization and pathogenic polyQ expansion is required for pathology in *Drosophila*. In contrast to HDL2-Q15, expression of HDL2-Q138 is highly toxic. Neuronal expression from the strongest HDL2 lines (generated through random P-element insertion) causes early pupal lethality, while low-expressing lines (generated from *attP2* site-direction insertion) are adult viable with progressive onset of motor defects and eventual lethality. This dose-dependent lethality agrees what has been observed in *Drosophila* HD models (13).

This study required the use of long polyQ repeat lengths within HDL2, as this accelerates toxicity and is needed for animals with short lifespans like *Drosophila*. The generation of animal models with CAG stretches longer than the median repeat length of the patient population is a

common approach in the polyQ field. For example, studies sampling thousands of HD patients have found the median *HTT* CAG repeat length is 43-46 (26–31). In contrast, most HD mouse models are generated using CAG lengths near or over 100 repeats, including the popular R6/2 model, which has a repeat length of around 150 (32–52). Similar ranges are found in *Drosophil*a models of HD, where pathogenic *HTT* constructs contain up to 152 repeats (13, 53–60). These animal models have accelerated onset of phenotypes, and may induce distinct pathologies than those observed in human neurons that have expressed the toxic protein for decades.

In *Drosophila* neurons, the cellular localization of HDL2-Q138 suggests mechanisms of toxicity are likely distinct from what we observed previously in an HD model we created. The *Drosophila* HD model used in these experiments contains a 588-amino acid fragment spanning exons 1 to 12 of the human *Htt* locus, which corresponds to a known cleavage product of full-length HTT. In neurons, HDL2-Q138 aggregates in the nucleus, often forming one large inclusion (Figs. 2B, 3A). This observation is similar to findings from HD and HDL2 patient brain tissue, where aggregated protein often forms one large nuclear inclusion, although multiple inclusions per nucleus are occasionally found (2, 61). The nuclear aggregation of HDL2-Q138 contrasts with several *Drosophila* models of HD, where pathogenic HTT remains confined to the cytoplasm (Figs. 2C, G, K, 3B) (13, 54, 56). Furthermore, while HTT-Q138 forms large axonal aggregates, HDL2-Q138 is trafficked down the axon as small puncta (Figs. 3D, E). Despite these differences in neurons, HDL2-Q138 and HTT-Q138 share a similar distribution pattern in epithelial cells of the salivary gland, where both form cytoplasmic aggregates (Figs. 2J, K). It will be interesting to determine if salivary glands lack important nuclear factors for HDL2 that normally trigger nuclear aggregation, or alternatively express cytoplasmic proteins that promote aggregation within this compartment before nuclear accumulation can occur. While these

findings represent data from one *Drosophila* HD model, it will be important to test additional disease-relevant HTT species in the future, including those where the protein is forced into the nucleus with an NLS tag. Furthermore, it is important to note that mutant HTT is not cleaved and processed in *Drosophila* the same way it is in mammalian neurons (13). It would therefore be worthwhile to study the similarities and differences between HDL2 and full-length HTT in mammalian models as well. Ultimately, modeling the polyQ diseases in a variety of systems will allow for deeper inquiry into mechanisms of toxicity.

In addition to differences from HTT-Q138, HDL2-Q138 localization is also distinct from a pure polyQ tract protein. While Q127 and HDL2-Q138 form nuclear aggregates in neurons, Q127 is not transported along axons (Figs. 2B, D, 3A, C, D, F). In muscle, both form nuclear aggregates, but HDL2-Q138 is also observed as puncta in the cytoplasm while Q127 is rarely observed outside of the nucleus (Figs. 2F, H). In epithelial cells of the salivary gland, HDL2-Q138 aggregates in the cytoplasm, while Q127 aggregates in the nucleus (Figs. 2J, L). As such, HDL2-Q138 appears distinct from either pathogenic HTT or an expanded polyQ tract in its aggregation pattern across a population of cell types in *Drosophila* (Table 1).

Distinctions between HDL2-Q138 and HTT-Q138 are also apparent at synapses of glutamatergic motor neurons. In our *Drosophila* HD model, HTT-Q138 accumulates locally at the NMJ and induces a synaptic overgrowth phenotype characterized by supernumerary satellite boutons (Fig. 3H). In contrast, HDL2-Q138 can be found as small puncta at the NMJ, but does not accumulate in appreciable quantities or form large aggregates (Fig. 3G). Neuronal expression of HDL2-Q138 does not lead to impaired synaptic function that we can measure through physiological analysis (Supplementary Material, Fig. S2). It is possible that physiological deficits are occurring in the central nervous system, or would appear at more mature synapses. Since

these experiments were conducted using a neuronal driver, only the presynaptic partner (the neuron) expressed HDL2-Q138, while the postsynaptic partner (the muscle) did not. Given HDL2-Q138 is expressed both pre- and post-synaptically, it will be interesting to examine postsynaptic effects of HDL2 expression in future studies.

Experiments redirecting HDL2 into or out of the nucleus demonstrate that nuclear mechanisms are critical to HDL2-Q138-induced toxicity. NES or NLS tagging redistributes the HDL2-Q138 protein to the desired compartment (Figs. 4B, E, H). This is important to note in light of research in HD models, where addition of NES tags reduce nuclear contribution of HTT, but some nuclear aggregates are still present (62, 63). The SV40 NLS sequence and modified PKI NES sequence used in our experiments alter the localization of all detectable HDL2 protein. The effect of nuclear localization or nuclear export of HDL2-Q138 is consistent across various tissues. Expression of an unmodified HDL2-Q138^{attP2} is not sufficient to cause eye degeneration, but targeting the protein to the nucleus induces a rough eye degenerative phenotype (Fig. 5). In muscle tissue, nuclear localization of HDL2-Q138 accelerates lethality, while nuclear export completely suppresses toxicity induced by the protein (Figs. 4C, F, I). In neurons, nuclear localization accelerates onset of motor dysfunction and significantly reduces lifespan compared to animals expressing the untagged HDL2-Q138^{attP2} (Fig. 6). Strikingly, motor function and lifespan are fully restored to control levels when the protein is confined to the cytoplasm. This complete suppression demonstrates that nuclear localization of an expanded HDL2 polyQ protein is required for the manifestation of pathology in the *Drosophila* model.

The importance of nuclear localization to HDL2 toxicity is interesting given that nuclear localization exacerbates toxicity in HD, but cytoplasmic mechanisms also play a role in pathogenesis. Addition of an NLS to HTT-Q144 accelerates onset of disease phenotypes in

transgenic mice. However, disease pathogenesis is not exclusively due to nuclear (*e.g.*, transcriptional) aberrations, as affected neurons have dark and degenerating organelles and swollen axons, indicating cytoplasmic dysfunction as well. Furthermore, addition of an NES tag to HTT-Q144 does not fully suppress mutant phenotypes (63). Similar results were obtained in *in vitro* experiments. Addition of an NLS tag to a fragment of HTT-Q75 doubled the percent of cells lost, while NES-tagged HTT-Q75 reduced cell loss, but did not fully suppress toxicity (62). Finally, multiple *Drosophila* models of HD display pathogenesis without nuclear localization of the pathogenic HTT protein, further demonstrating that cytoplasmic mechanisms are sufficient to induce toxicity in these HD models (13, 54, 56). These data demonstrate that although nuclear localization of mutant HTT is detrimental, both nuclear and cytoplasmic events contribute to pathogenesis. This contrasts with our findings for pathogenic HDL2, which induces toxicity only when the protein accumulates in the nucleus.

The toxic contribution of nuclear versus cytoplasmic protein load has also been studied in other polyQ disease models. Similar to what has been observed in HD, nuclear localization exacerbates phenotypes in MJD model mice. However, nuclear export does not completely suppress toxicity (64). In contrast, nuclear localization is essential for toxicity in SCA1. In transgenic mouse models of SCA1, expanded ataxin-1 localizes to the nucleus, and animals exhibit motor defects followed by atrophy or loss of Purkinje cells (65, 66). When expanded ataxin-1 is blocked from nuclear entry, toxicity is fully suppressed, with no apparent behavioral defects or neuropathology (67). Nuclear mechanisms are also important to disease pathogenesis in dentatorubro-pallidoluysian atrophy (DRPLA). DRPLA patients and transgenic mouse models present with nuclear accumulation of atrophin-1. Cell culture experiments show that directing expanded atrophin-1 to the nucleus increases toxicity, while mutating the NLS restores cell loss

to control levels (68). Nuclear localization is not required for toxicity in all polyQ diseases. In the case of spinocerebellar ataxia 2 (SCA2), pathology occurs without nuclear ataxin-2 protein. In contrast to patients with HDL2, HD, SCA1, or MJD, postmortem brain tissue from patients with SCA2 does not reveal polyQ neuronal nuclear inclusion, nor is expanded ataxin-2 observed in the nucleus in a SCA2 mouse model (69). Current hypotheses suggest SCA2 pathogenesis may arise from impaired calcium signaling or dysfunctional RNA regulation and transport, but the mechanisms of cellular toxicity remain unclear (70–73).

While HDL2 patients' symptoms and neuropathology mimic HD, dysfunction at the molecular level may be reminiscent of another polyQ disorder, SCA1, where nuclear localization of the pathogenic protein is required for toxicity. The mechanism of nuclear toxicity in HDL2 remains an open question. Staining with anti-fibrillarin demonstrates that the expanded HDL2-Q138 protein does not localize to the nucleolus (Supplementary Material, Fig. S3). This observation matches findings from brain tissue of patients with HD, DRPLA, SCA1, and MJD, where the polyQ proteins tend to form single large inclusions that remain distinct from the nucleolus (61, 74–76). Also, FRAP experiments suggest that HDL2-Q138 does not appear to alter nuclear transport (Supplementary Material, Fig. S4), a pathogenic mechanism that is emerging in models of FTDALS1 (22–24).

There are a variety of mechanisms by which nuclear localization of pathogenic HDL2 may exert toxicity. One potential mechanism is transcriptional dysregulation, a well-established pathogenic pathway in the polyQ disorders (suggested reviews: J. H. J. Cha, 2007; J. H. Cha, 2000; Riley & Orr, 2006; Sugars & Rubinsztein, 2003). A comprehensive transcriptional profiling of HDL2 mutant animals via RNA sequencing could provide a starting point to delve deeper into mechanisms of polyQ toxicity in HDL2. Similarly, epigenetic changes may play a

role in HDL2 pathogenesis. This pathway that has been studied in depth in polyQ diseases, trinucleotide repeat expansion disorders, and other neurodegenerative diseases, such as Alzheimer's and Parkinson's (81–86). It also represents an attractive therapeutic approach given several pharmacological agents are available to modify epigenetic state (such as histone deacetylase inhibitors). Since DNA damage has been established as playing a role in a variety of neurodegenerative diseases, HDL2 nuclear localization could also disrupt this process (87–90). HDL2 nuclear aggregates or monomers could sequester or otherwise interfere with other nuclear proteins. For example, experiments in a SCA1 models show that expanded ataxin-1 causes a redistribution of the nuclear matrix-associated domain containing promyelocytic leukaemia protein (75).

The cause of human pathology in HDL2 remains an open question. Several pathogenic pathways have experimental support in the field, including *JPH3* loss of function, CUG RNA toxicity, and polyQ toxicity (91). Evidence from both HDL2 mouse models and HDL2 patient brain tissue suggest a polyQ protein may be involved in disease pathology. First, an antisense CAG transcript has been identified in human brain tissue (normal repeat length transcript) and an HDL2 mouse model (expanded length transcript) (4, 10). While the full-length transcript has not been isolated from human patient brain tissue, the possibility remains that the transcript is produced in neuronal populations other than frontal cortex, the only brain area tested (4). The nature of neurodegenerative diseases makes this a particularly difficult technical method, since the main neuronal populations of interest have been lost to disease. Additional evidence supporting a polyQ pathology comes from the observation that ubiquitinated neuronal inclusions have been found in human HDL2 patient brain tissue, as well as brain tissue from the HDL2 mouse models (2, 10). Immunohistochemistry on human patient and mouse model brain sections

have confirmed the inclusions can be stained with 1C2, an antibody that recognizes polyQ proteins. Inclusions in the mouse model were also tested with the 3B5H10 antibody, a more specific polyQ antibody (10). Hence, the multimodal pathogenesis of HDL2 may involve contribution from a toxic polyQ protein (91, 92), although other mechanisms likely contribute to the disease mechanism as well.

In conclusion, these experiments demonstrate that nuclear localization of the HDL2 polyQ protein is required for pathogenesis in a *Drosophila* model of the disorder. This contrasts with a *Drosophila* HD model expressing an N-terminal fragment of HTT, where toxicity occurs through cytoplasmic mechanisms. Confining HDL2-Q138 to the cytoplasm completely suppresses toxicity in a variety of tissue types tested, including neurons. In addition, nuclear export restores motor function and lifespan to control levels. In contrast, adding a NLS to HDL2-Q138 enhances pathology and decreases lifespan compared to unmodified HDL2-Q138. Thus, although similar neurological profiles are found in HD and HDL2 patients, HDL2 pathology may principally occur due to its accumulation within the nucleus. This contrasts with HD, where both nuclear and cytoplasmic pathology has been well documented. Additional research comparing our HDL2 *Drosophila* model with other *Drosophila* models of HD, along with comparing these polyQ proteins in mammalian models, may provide insight into mechanisms of toxicity and reveal additional similarities and differences between HD and HDL2.

Materials and methods

JPH3 antisense (HDL2) gene synthesis

Sequences were selected based on transcripts identified by 5' RACE experiments in BAC-HDL2 model mice (4, 10). The full-length isoform was used in these experiments. No HGNC-approved gene symbols have been determined for the antisense *CAG* product. The antisense gene at the *JPH3* locus that contributes to toxicity in HDL2 is referred to as *HDL2*, and the polyQ protein product as HDL2. *HDL2* constructs with either 15 or 138 CAG repeats (*HDL2-Q15*, *HDL2-Q138*) were synthesized and cloned into the pENTR1A Gateway® entry vector by Epoch Life Science.

Drosophila stocks and transgenics

All *Drosophila* strains were cultured on standard media at 25°C. *GAL4* driver lines (*elav, mef2, pickpocket*) and GFP control lines (*UAS-GFP, UAS-GFP-NLS*) were obtained from the Bloomington *Drosophila* Stock Center. Generation of HD model flies was described previously (13). To generate flies carrying *HDL2* transgenes at random insertion sites, *HDL2-Q15* and -*Q138* in pENTR1A were cloned into pUASt vectors pTRW, pTGW, and pTW (*Drosophila* Genomics Resource Center) using the Gateway® cloning system. Constructs were injected into *Drosophila* embryos (genotype w^{1118}) by BestGene. High expression lines selected for analysis were mapped to the third chromosome (BestGene). For nuclear localization and nuclear export experiments, *HDL2* constructs were modified at the 3' end with the addition of NLS (CCTAAGAAGAAGAGGAAGGTT) or NES (AACATTAACGAACTGGCGCTGAAATTTGCGGGCCTGGATATT) sequences. Using the Gateway® system, constructs were cloned into the pPGW (*Drosophila* Genomics Resource

Center) vector and injected into *Drosophila* embryos (genotype y^1 w^{67c23}; *P{CaryP}attP2*) by BestGene.

Immunohistochemistry

Wandering 3rd instar larvae reared at 25°C and dissected in HL3.1 solution, containing (in mM): 70 NaCl, 5 KCl, 4 $MgCl_2$, 10 $NaHCO_3$, 5 Trehalose, 115 sucrose, 5 HEPES-NaOH, pH 7.2, and 0.2 Ca^{++}. Larvae were fixed for 30 minutes in 4% formaldehyde, permeabilized for 30 minutes in 0.1% Triton-X100 in PBS (PBX), and blocked for 1 hour in 2% normal goat serum in PBX. The following antibodies were used: rat anti-elav (DSHB), mouse anti-lamin C (DSHB), FITC conjugated rabbit anti-HA (Abcam), Alexa Fluor® 647 goat anti-HRP (Jackson ImmunoResearch), Alexa Fluor® 405 goat anti-rat (Abcam), Alexa Fluor® 405 goat anti-mouse (Life Technologies). Larvae were mounted in Vectashield® antifade mounting medium or Vectashield® antifade mounting medium with DAPI (Vector Laboratories). Images were captured with a Zeiss Pascal laser scanning confocal microscope (Carl Zeiss MicroImaging, Inc.) using the accompanying Zeiss PASCAL software or a spinning disk confocal microscope (Carl Zeiss MicroImaging, Inc.) using Perkin Elmer Volocity software.

Eye imaging

Drosophila eyes were photographed using a Zeiss Stemi 2000-C stereo microscope (Carl Zeiss MicroImaging, Inc.) fitted with a SPOT idea CMOS camera (SPOT Imaging) and captured with the accompanying SPOT Imaging software.

Lifespan assay

Drosophila viability assays were performed on male flies aged at 29°C, with 10 flies per vial, and transferred every 2-3 days. 50 flies per genotype were used.

Climbing assay

Male *Drosophila* were aged at 29°C, with no more than 10 flies per vial, and transferred every 2-3 days. At age 1 day, 1 week, 3 weeks, and 5 weeks, flies were transferred to empty vials and left to recover for one hour at room temperature. Flies were then briefly vortexed to knock them all to the bottom of the vial and their subsequent climbing was recorded. The percent of flies climbing above 2 cm in 30 seconds was used for analysis. 50 flies per genotype were used.

Statistical analysis

Analysis of variance (ANOVA) with Tukey's post-hoc test (Fig. 6A), and the Mantel-Cox test (Fig. 6B) were used to determine statistical significance using Prism software (GraphPad).

OMIM reference numbers

Online Mendelian Inheritance in Man (http://www.ncbi.nlm.nih.gov/omim) reference numbers for the disorders described in this paper are as follows: dentatorubro-pallidoluysian atrophy (#125370), frontotemporal dementia and/or amyotrophic lateral sclerosis 1 (#105550), Huntington disease (#143100), Huntington disease-like 2 (#606438), Machado-Joseph disease (#109150), myotonic dystrophy 1 (#160900), spinocerebellar ataxia 1 (#164400), spinocerebellar ataxia 2 (#183090), spinocerebellar ataxia 8 (#608768).

Acknowledgements

We thank Kayla Brown, Kendall Kiser, Ryan Littleton, Dina Volfsen and Kathyrn Harris for experimental help. This work was supported by the National Institutes of Health (grant number NS40296, MH104536) and the JPB Foundation. Stocks obtained from the Bloomington *Drosophila* Stock Center (funded by National Institutes of Health grant P40OD018537) were used in this study. The antibodies against elav (developed by G. M. Rubin) and lamin C (deposited by P. A. Fisher) were obtained from the Developmental Studies Hybridoma Bank, created by the Eunice Kennedy Shriver National Institute of Child Health and Human Development of the National Institutes of Health and maintained at the University of Iowa, Department of Biology, Iowa City, IA 52242. We thank the *Drosophila* Genomics Resource Center (supported by National Institutes of Health grant 2P40OD010949-10A1) for vectors (deposited by T. Murphy).

Conflict of Interest Statement

The authors declare no competing interests.

References

1. Margolis, R.L., Rudnicki, D.D. and Holmes, S.E. (2005) Huntington's Disease Like-2 : Review and Update. *Acta Neurol. Taiwan.*, **14**, 1–8.

2. Rudnicki, D.D., Pletnikova, O., Vonsattel, J.P.G., Ross, C.A. and Margolis, R.L. (2008) A comparison of Huntington disease and Huntington disease-like 2 neuropathology. *J. Neuropathol. Exp. Neurol.*, **67**, 366–374.

3. Holmes, S.E., O'Hearn, E., Rosenblatt, A., Callahan, C., Hwang, H.S., Ingersoll-Ashworth, R.G., Fleisher, A., Stevanin, G., Brice, A., Potter, N.T., *et al.* (2001) A repeat expansion in the gene encoding junctophilin-3 is associated with Huntington disease-like 2. *Nat. Genet.*, **29**, 377–378.

4. Seixas, A.I., Holmes, S.E., Takeshima, H., Pavlovich, A., Sachs, N., Pruitt, J.L., Silveira, I., Ross, C.A., Margolis, R.L. and Rudnicki, D.D. (2012) Loss of junctophilin-3 contributes to huntington disease-like 2 pathogenesis. *Ann. Neurol.*, **71**, 245–257.

5. Li, L.B., Yu, Z., Teng, X. and Bonini, N.M. (2008) RNA toxicity is a component of ataxin-3 degeneration in Drosophila. *Nature*, **453**, 1107–1111.

6. Koob, M.D., Moseley, M.L., Schut, L.J., Benzow, K.A., Bird, T.D., Day, J.W. and Ranum, L.P. (1999) An untranslated CTG expansion causes a novel form of spinocerebellar ataxia (SCA8). *Nat. Genet.*, **21**, 379–384.

7. Jiang, H., Mankodi, A., Swanson, M.S., Moxley, R.T. and Thornton, C.A. (2004) Myotonic dystrophy type 1 is associated with nuclear foci of mutant RNA, sequestration of muscleblind proteins and deregulated alternative splicing in neurons. *Hum. Mol. Genet.*, **13**, 3079–3088.

8. Rudnicki, D.D., Holmes, S.E., Lin, M.W., Thornton, C. a., Ross, C. a. and Margolis, R.L. (2007) Huntington's disease-like 2 is associated with CUG repeat-containing RNA foci. *Ann. Neurol.*, **61**, 272–282.

9. Moseley, M.L., Zu, T., Ikeda, Y., Gao, W., Mosemiller, A.K., Daughters, R.S., Chen, G., Weatherspoon, M.R., Clark, H.B., Ebner, T.J., *et al.* (2006) Bidirectional expression of CUG and CAG expansion transcripts and intranuclear polyglutamine inclusions in spinocerebellar ataxia type 8. *Nat. Genet.*, **38**, 758–769.

10. Wilburn, B., Rudnicki, D.D., Zhao, J., Weitz, T.M., Cheng, Y., Gu, X., Greiner, E., Park, C.S., Wang, N., Sopher, B.L., *et al.* (2011) An antisense CAG repeat transcript at JPH3 locus mediates expanded polyglutamine protein toxicity in Huntington's disease-like 2 mice. *Neuron*, **70**, 427–440.

11. Batra, R., Charizanis, K. and Swanson, M.S. (2010) Partners in crime: Bidirectional transcription in unstable microsatellite disease. *Hum. Mol. Genet.*, **19**, 77–82.

12. He, Y., Vogelstein, B., Velculescu, V.E., Papadopoulos, N. and Kinzler, K.W. (2008) The antisense transcriptomes of human cells. *Science*, **322**, 1855–1857.

13. Weiss, K.R., Kimura, Y., Lee, W.C.M. and Littleton, J.T. (2012) Huntingtin aggregation kinetics and their pathological role in a Drosophila Huntington's disease model. *Genetics*, **190**, 581–600.

14. Kazemi-Esfarjani, P. and Benzer, S. (2000) Genetic suppression of polyglutamine toxicity in Drosophila. *Science*, **287**, 1837–1840.

15. Wellington, C.L., Ellerby, L.M., Gutekunst, C.A., Rogers, D., Warby, S., Graham, R.K., Loubser, O., van Raamsdonk, J., Singaraja, R., Yang, Y.Z., *et al.* (2002) Caspase cleavage

of mutant huntingtin precedes neurodegeneration in Huntington's disease. *J. Neurosci.*, **22**, 7862–7872.

16. Gafni, J., Hermel, E., Young, J.E., Wellington, C.L., Hayden, M.R. and Ellerby, L.M. (2004) Inhibition of calpain cleavage of huntingtin reduces toxicity: Accumulation of calpain/caspase fragments in the nucleus. *J. Biol. Chem.*, **279**, 20211–20220.

17. Lunkes, A., Lindenberg, K.S., Ben-Haem, L., Weber, C., Devys, D., Landwehrmeyer, G.B., Mandel, J.L. and Trottier, Y. (2002) Proteases acting on mutant huntingtin generate cleaved products that differentially build up cytoplasmic and nuclear inclusions. *Mol. Cell*, **10**, 259–269.

18. Kim, Y.J., Yi, Y., Sapp, E., Wang, Y., Cuiffo, B., Kegel, K.B., Qin, Z.H., Aronin, N. and DiFiglia, M. (2001) Caspase 3-cleaved N-terminal fragments of wild-type and mutant huntingtin are present in normal and Huntington's disease brains, associate with membranes, and undergo calpain-dependent proteolysis. *Proc. Natl. Acad. Sci. U. S. A.*, **98**, 12784–12789.

19. Oh, E. and Robinson, I. (2012) Barfly: Sculpting membranes at the Drosophila neuromuscular junction. *Dev. Neurobiol.*, **72**, 33–56.

20. Lam, Y.W. and Trinkle-Mulcahy, L. (2015) New insights into nucleolar structure and function. *F1000Prime Rep.*, 10.12703/P7-48.

21. Peng, J.C. and Karpen, G.H. (2007) H3K9 methylation and RNA interference regulate nucleolar organization and repeated DNA stability. *Nat. Cell Biol.*, **9**, 25–35.

22. Freibaum, B.D., Lu, Y., Lopez-Gonzalez, R., Kim, N.C., Almeida, S., Lee, K.H., Badders, N., Valentine, M., Miller, B.L., Wong, P.C., *et al.* (2015) GGGGCC repeat expansion in

C9orf72 compromises nucleocytoplasmic transport. *Nature*, **525**, 129–133.

23. Zhang, K., Donnelly, C.J., Haeusler, A.R., Grima, J.C., Machamer, J.B., Steinwald, P., Daley, E.L., Miller, S.J., Cunningham, K.M., Vidensky, S., *et al.* (2015) The C9orf72 repeat expansion disrupts nucleocytoplasmic transport. *Nature*, **525**, 56–61.

24. Jovic, A., Mertens, J. and Boeynaems, S. (2015) Modifiers of C9orf72 dipeptide repeat toxicity connect nucleocytoplasmic transport defects to FTD / ALS. *Nat. Neurosci.*, **18**, 1226–1229.

25. Jackson, G.R. (2008) Guide to understanding Drosophila models of neurodegenerative diseases. *PLoS Biol.*, **6**, 0236–0239.

26. Maat-Kievit, A., Losekoot, M., Zwinderman, K., Vegter-van der Vlis, M., Belfroid, R., Lopez, F., van Ommen, G.-J., Breuning, M. and Roos, R. (2002) Predictability of Age at Onset in Huntington Disease in the Dutch Population. *Medicine (Baltimore).*, **81**, 251–259.

27. Andrew, S.E., Goldberg, Y.P., Kremer, B., Telenius, H., Theilmann, J., Adam, S., Starr, E., Squitieri, F., Lin, B. and Kalchman, M. a (1993) The relationship between trinucleotide (CAG) repeat length and clinical features of Huntington's disease. *Nat. Genet.*, **4**, 398–403.

28. Lucotte, G., Turpin, J.C., Riess, O., Epplen, J.T., Siedlaczk, I., Loirat, F. and Hazout, S. (1995) Confidence intervals for predicted age of onset, given the size of (CAG)n repeat, in Huntington's disease. *Hum. Genet.*, **95**, 231–232.

29. Barron, L.H., Warner, J.P., Porteous, M., Holloway, S., Simpson, S., Davidson, R. and Brock, D.J. (1993) A study of the Huntington's disease associated trinucleotide repeat in the Scottish population. *J Med Genet*, **30**, 1003–1007.

30. Langbehn, D.R., Brinkman, R.R., Falush, D., Paulsen, J.S. and Hayden, M.R. (2004) A new model for prediction of the age of onset and penetrance for Huntington's disease based on CAG length. *Clin. Genet.*, **65**, 267–277.

31. Squitieri, F., Sabbadini, G., Mandich, P., Gellera, C., Di Maria, E., Bellone, E., Castellotti, B., Nargi, E., De Grazia, U., Frontali, M., *et al.* (2000) Family and molecular data for a fine analysis of age at onset in Huntington disease. *Am. J. Med. Genet.*, **95**, 366–373.

32. Mangiarini, L., Sathasivam, K., Seller, M., Cozens, B., Harper, A., Hetherington, C., Lawton, M., Trottier, Y., Lehrach, H., Davies, S.W., *et al.* (1996) Exon I of the HD gene with an expanded CAG repeat is sufficient to cause a progressive neurological phenotype in transgenic mice. *Cell*, **87**, 493–506.

33. Carter, R.J., Lione, L.A., Humby, T., Mangiarini, L., Mahal, A., Bates, G.P., Dunnett, S.B. and Morton, A.J. (1999) Characterization of progressive motor deficits in mice transgenic for the human Huntington's disease mutation. *J. Neurosci.*, **19**, 3248–3257.

34. Hodges, A., Hughes, G., Brooks, S., Elliston, L., Holmans, P., Dunnett, S.B. and Jones, L. (2008) Brain gene expression correlates with changes in behavior in the R6/1 mouse model of Huntington's disease. *Genes, Brain Behav.*, **7**, 288–299.

35. Schilling, G., Becher, M.W., Sharp, A.H., Jinnah, H.A., Duan, K., Kotzuk, J.A., Slunt, H.H., Ratovitski, T., Cooper, J.K., Jenkins, N.A., *et al.* (1999) Intranuclear inclusions and neuritic aggregates in transgenic mice expressing a mutant N-terminal fragment of huntingtin. *Hum. Mol. Genet.*, **8**, 397–407.

36. Schilling, G., Savonenko, A. V., Coonfield, M.L., Morton, J.L., Vorovich, E., Gale, A., Neslon, C., Chan, N., Eaton, M., Fromholt, D., *et al.* (2004) Environmental,

pharmacological, and genetic modulation of the HD phenotype in transgenic mice. *Exp. Neurol.*, **187**, 137–149.

37. Laforet, G.A., Sapp, E., Chase, K., McIntyre, C., Boyce, F.M., Campbell, M., Cadigan, B.A., Warzecki, L., Tagle, D.A., Reddy, P.H., *et al.* (2001) Changes in cortical and striatal neurons predict behavioral and electrophysiological abnormalities in a transgenic murine model of Huntington's disease. *J. Neurosci.*, **21**, 9112–9123.

38. Yamamoto, a, Lucas, J.J. and Hen, R. (2000) Reversal of neuropathology and motor dysfunction in a conditional model of Huntington's disease. *Cell*, **101**, 57–66.

39. Hodgson, J.G., Agopyan, N., Gutekunst, C.A., Leavitt, B.R., Lepiane, F., Singaraja, R., Smith, D.J., Bissada, N., McCutcheon, K., Nasir, J., *et al.* (1999) A YAC mouse model for Huntington's disease with full-length mutant huntingtin, cytoplasmic toxicity, and selective striatal neurodegeneration. *Neuron*, **23**, 181–192.

40. Seo, H., Kim, W. and Isacson, O. (2008) Compensatory changes in the ubiquitin-proteasome system, brain-derived neurotrophic factor and mitochondrial complex II/III in YAC72 and R6/2 transgenic mice partially model Huntington's disease patients. *Hum. Mol. Genet.*, **17**, 3144–3153.

41. Slow, E.J., van Raamsdonk, J., Rogers, D., Coleman, S.H., Graham, R.K., Deng, Y., Oh, R., Bissada, N., Hossain, S.M., Yang, Y.Z., *et al.* (2003) Selective striatal neuronal loss in a YAC128 mouse model of Huntington disease. *Hum. Mol. Genet.*, **12**, 1555–1567.

42. Gray, M., Shirasaki, D.I., Cepeda, C., Andre, V.M., Wilburn, B., Lu, X.H., Tao, J., Yamazaki, I., Li, S.H., Sun, Y.E., *et al.* (2008) Full-length human mutant huntingtin with a stable polyglutamine repeat can elicit progressive and selective neuropathogenesis in

BACHD mice. *J Neurosci*, **28**, 6182–6195.

43. Shelbourne, P.F., Killeen, N., Hevner, R.F., Johnston, H.M., Tecott, L., Lewandoski, M., Ennis, M., Ramirez, L., Li, Z., Iannicola, C., *et al.* (1999) A Huntington's disease CAG expansion at the murine Hdh locus is unstable and associated with behavioural abnormalities in mice. *Hum. Mol. Genet.*, **8**, 763–774.

44. Kennedy, L., Evans, E., Chen, C.M., Craven, L., Detloff, P.J., Ennis, M. and Shelbourne, P.F. (2003) Dramatic tissue-specific mutation length increases are an early molecular event in Huntington disease pathogenesis. *Hum. Mol. Genet.*, **12**, 3359–3367.

45. Wheeler, V.C., Auerbach, W., White, J.K., Srinidhi, J., Auerbach, A., Ryan, A., Duyao, M.P., Vrbanac, V., Weaver, M., Gusella, J.F., *et al.* (1999) Length-dependent gametic CAG repeat instability in the Huntington's disease knock-in mouse. *Hum. Mol. Genet.*, **8**, 115–122.

46. Wheeler, V.C., Gutekunst, C.-A., Vrbanac, V., Lebel, L.-A., Schilling, G., Hersch, S., Friedlander, R.M., Gusella, J.F., Vonsattel, J.-P., Borchelt, D.R., *et al.* (2002) Early phenotypes that presage late-onset neurodegenerative disease allow testing of modifiers in Hdh CAG knock-in mice. *Hum. Mol. Genet.*, **11**, 633–40.

47. Levine, M.S., Klapstein, G.J., Koppel, A., Gruen, E., Cepeda, C., Vargas, M.E., Jokel, E.S., Carpenter, E.M., Zanjani, H., Hurst, R.S., *et al.* (1999) Enhanced sensitivity to N-methyl-D-aspartate receptor activation in transgenic and knockin mouse models of Huntington's disease. *J Neurosci Res*, **58**, 515–532.

48. Menalled, L.B., Sison, J.D., Wu, Y., Olivieri, M., Li, X.-J., Li, H., Zeitlin, S. and Chesselet, M.-F. (2002) Early motor dysfunction and striosomal distribution of huntingtin

microaggregates in Huntington's disease knock-in mice. *J. Neurosci.*, **22**, 8266–8276.

49. Menalled, L.B., Sison, J.D., Dragatsis, I., Zeitlin, S. and Chesselet, M.F. (2003) Time course of early motor and neuropathological anomalies in a knock-in mouse model of Huntington's disease with 140 CAG repeats. *J. Comp. Neurol.*, **465**, 11–26.

50. Hickey, M.A., Kosmalska, A., Enayati, J., Cohen, R., Zeitlin, S., Levine, M.S. and Chesselet, M.F. (2008) Extensive early motor and non-motor behavioral deficits are followed by striatal neuronal loss in knock-in Huntington's disease mice. *Neuroscience*, **157**, 280–295.

51. Lin, C.H., Tallaksen-Greene, S., Chien, W.M., Cearley, J.A., Jackson, W.S., Crouse, A.B., Ren, S., Li, X.J., Albin, R.L. and Detloff, P.J. (2001) Neurological abnormalities in a knock-in mouse model of Huntington's disease. *Hum. Mol. Genet.*, **10**, 137–44.

52. Heng, M.Y., Tallaksen-Greene, S.J., Detloff, P.J. and Albin, R.L. (2007) Longitudinal evaluation of the Hdh(CAG)150 knock-in murine model of Huntington's disease. *J Neurosci*, **27**, 8989–8998.

53. Jackson, G.R., Salecker, I., Dong, X., Yao, X., Arnheim, N., Faber, P.W., MacDonald, M.E. and Zipursky, S.L. (1998) Polyglutamine-expanded human huntingtin transgenes induce degeneration of Drosophila photoreceptor neurons. *Neuron*, **21**, 633–642.

54. Romero, E., Cha, G.H., Verstreken, P., Ly, C.V., Hughes, R.E., Bellen, H.J. and Botas, J. (2008) Suppression of neurodegeneration and increased neurotransmission caused by expanded full-length huntingtin accumulating in the cytoplasm. *Neuron*, **57**, 27–40.

55. Doumanis, J., Wada, K., Kino, Y., Moore, A.W. and Nukina, N. (2009) RNAi screening in Drosophila cells identifies new modifiers of mutant huntingtin aggregation. *PLoS One*, **4**, e7275.

56. Lee, W.C.M., Yoshihara, M. and Littleton, J.T. (2004) Cytoplasmic aggregates trap polyglutamine-containing proteins and block axonal transport in a Drosophila model of Huntington's disease. *Proc. Natl. Acad. Sci. U. S. A.*, **101**, 3224–3229.

57. Steffan, J.S., Bodai, L., Pallos, J., Poelman, M., McCampbell, A., Apostol, B.L., Kazantsev, A., Schmidt, E., Zhu, Y.Z., Greenwald, M., *et al.* (2001) Histone deacetylase inhibitors arrest polyglutamine-dependent neurodegeneration in Drosophila. *Nature*, **413**, 739–743.

58. Kaltenbach, L.S., Romero, E., Becklin, R.R., Chettier, R., Bell, R., Phansalkar, A., Strand, A., Torcassi, C., Savage, J., Hurlburt, A., *et al.* (2007) Huntingtin interacting proteins are genetic modifiers of neurodegeneration. *PLoS Genet.*, **3**, e82.

59. Zhang, S., Binari, R., Zhou, R. and Perrimon, N. (2010) A genomewide RNA interference screen for modifiers of aggregates formation by mutant huntingtin in *Drosophila*. *Genetics*, **184**, 1165–1179.

60. Schulte, J., Sepp, K.J., Wu, C., Hong, P. and Littleton, J.T. (2011) High-content chemical and RNAi screens for suppressors of neurotoxicity in a Huntington's disease model. *PLoS One*, **6**, e23841.

61. DiFiglia, M., Sapp, E., Chase, K.O., Davies, S.W., Bates, G.P., Vonsattel, J.P. and Aronin, N. (1997) Aggregation of huntingtin in neuronal intranuclear inclusions and dystrophic neurites in brain. *Science*, **277**, 1990–1993.

62. Peters, M.F., Nucifora, F.C., Kushi, J., Seaman, H.C., Cooper, J.K., Herring, W.J., Dawson, V.L., Dawson, T.M. and Ross, C.A. (1999) Nuclear targeting of mutant huntingtin increases toxicity. *Mol. Cell. Neurosci.*, **14**, 121–128.

63. Benn, C.L., Landles, C., Li, H., Strand, A.D., Woodman, B., Sathasivam, K., Li, S.H., Ghazi-

Noori, S., Hockly, E., Faruque, S.M.N.N., *et al.* (2005) Contribution of nuclear and extranuclear polyQ to neurological phenotypes in mouse models of Huntington's disease. *Hum. Mol. Genet.*, **14**, 3065–3078.

64. Bichelmeier, U., Schmidt, T., Hübener, J., Boy, J., Rüttiger, L., Häbig, K., Poths, S., Bonin, M., Knipper, M., Schmidt, W.J., *et al.* (2007) Nuclear localization of ataxin-3 is required for the manifestation of symptoms in SCA3: in vivo evidence. *J. Neurosci.*, **27**, 7418–7428.

65. Burright, E.N., Clark, H.B., Servadio, A., Matilla, T., Feddersen, R.M., Yunis, W.S., Duvick, L.A., Zoghbi, H.Y. and Orr, H.T. (1995) SCA1 transgenic mice: a model for neurodegeneration caused by an expanded CAG trinucleotide repeat. *Cell*, **82**, 937–948.

66. Clark, H., Burright, E., Yunis, W., Larson, S., Wilcox, C., Hartman, B., Matilla, A., Zoghbi, H. and Orr, H. (1997) Purkinje cell expression of a mutant allele of SCA1 in transgenic mice leads to disparate effects on motor behaviors, followed by a progressive cerebellar dysfunction and histological alterations. *J. Neurosci.*, **17**, 7385–7395.

67. Klement, I.A., Skinner, P.J., Kaytor, M.D., Yi, H., Hersch, S.M., Clark, H.B., Zoghbi, H.Y. and Orr, H.T. (1998) Ataxin-1 nuclear localization and aggregation: Role in polyglutarnine-induced disease in SCA1 transgenic mice. *Cell*, **95**, 41–53.

68. Nucifora, F.C., Ellerby, L.M., Wellington, C.L., Wood, J.D., Herring, W.J., Sawa, A., Hayden, M.R., Dawson, V.L., Dawson, T.M. and Ross, C.A. (2003) Nuclear localization of a non-caspase truncation product of atrophin-1, with an expanded polyglutamine repeat, increases cellular toxicity. *J. Biol. Chem.*, **278**, 13047–13055.

69. Huynh, D.P., Figueroa, K., Hoang, N. and Pulst, S.M. (2000) Nuclear localization or inclusion body formation of ataxin-2 are not necessary for SCA2 pathogenesis in mouse or

human. *Nat. Genet.*, **26**, 44–50.

70. Satterfield, T.F., Jackson, S.M. and Pallanck, L.J. (2002) A Drosophila homolog of the polyglutamine disease gene SCA2 is a dosage-sensitive regulator of actin filament formation. *Genetics*, **162**, 1687–702.

71. Kiehl, T.R., Shibata, H., Vo, T., Huynh, D.P. and Pulst, S.M. (2001) Identification and expression of a mouse ortholog of A2BP1. *Mamm. Genome*, **12**, 595–601.

72. Shibata, H., Huynh, D.P. and Pulst, S.M. (2000) A novel protein with RNA-binding motifs interacts with ataxin-2. *Hum. Mol. Genet.*, **9**, 1303–1313.

73. Liu, J., Tang, T.-S., Tu, H., Nelson, O., Herndon, E., Huynh, D.P., Pulst, S.M. and Bezprozvanny, I. (2009) Deranged Calcium Signaling and Neurodegeneration in Spinocerebellar Ataxia Type 2. *J. Neurosci.*, **29**, 9148–9162.

74. Becher, M.W., Kotzuk, J.A., Sharp, A.H., Davies, S.W., Bates, G.P., Price, D.L. and Ross, C.A. (1998) Intranuclear neuronal inclusions in Huntington's disease and dentatorubral and pallidoluysian atrophy: correlation between the density of inclusions and IT15 CAG triplet repeat length. *Neurobiol. Dis.*, **4**, 387–397.

75. Skinner, P.J., Koshy, B.T., Cummings, C.J., Klement, I.A., Helin, K., Servadio, A., Zoghbi, H.Y. and Orr, H.T. (1997) Ataxin-1 with an expanded glutamine tract alters nuclear matrix-associated structures. *Nature*, **389**, 971–974.

76. Paulson, H.L., Perez, M.K., Trottier, Y., Trojanowski, J.Q., Subramony, S.H., Das, S.S., Vig, P., Mandel, J.L., Fischbeck, K.H. and Pittman, R.N. (1997) Intranuclear inclusions of expanded polyglutamine protein in spinocerebellar ataxia type 3. *Neuron*, **19**, 333–344.

77. Sugars, K.L. and Rubinsztein, D.C. (2003) Transcriptional abnormalities in Huntington disease. *Trends Genet.*, **19**, 233–238.

78. Cha, J.H.J. (2000) Transcriptional dysregulation in Huntington's disease. *Trends Neurosci*, **23**, 387–392.

79. Cha, J.H.J. (2007) Transcriptional signatures in Huntington's disease. *Prog. Neurobiol.*, **83**, 228–248.

80. Riley, B.E. and Orr, H.T. (2006) Polyglutamine neurodegenerative diseases and regulation of transcription: Assembling the puzzle. *Genes Dev.*, **20**, 2183–2192.

81. Valor, L.M., Guiretti, D., Lopez-Atalaya, J.P. and Barco, A. (2013) Genomic landscape of transcriptional and epigenetic dysregulation in early onset polyglutamine disease. *J. Neurosci.*, **33**, 10471–10482.

82. Cohen-Carmon, D. and Meshorer, E. (2012) Polyglutamine (polyQ) disorders: The chromatin connection. *Nucleus*, **3**, 433–441.

83. Lord, J. and Cruchaga, C. (2014) The epigenetic landscape of Alzheimer's disease. *Nat. Neurosci.*, **17**, 1138–1140.

84. Harrison, I.F. and Dexter, D.T. (2013) Epigenetic targeting of histone deacetylase: Therapeutic potential in Parkinson's disease? *Pharmacol. Ther.*, **140**, 34–52.

85. Wang, J., Yu, J.T., Tan, M.S., Jiang, T. and Tan, L. (2013) Epigenetic mechanisms in Alzheimer's disease: Implications for pathogenesis and therapy. *Ageing Res. Rev.*, **12**, 1024–1041.

86. Fang, H. and Todd, P.K. (2011) Epigenetic Mechanisms in Repeat Expansion Disorders.

Semin. Neurol., **31**, 470–483.

87. Coppedè, F. and Migliore, L. (2015) DNA damage in neurodegenerative diseases. *Mutat. Res. Mol. Mech. Mutagen.*, **776**, 84–97.

88. Okazawa, H. (2011) DNA repair and neurodegeneration: a common pathology shared by polyglutamine diseases. *Rinsho Shinkeigaku*, **51**, 979–981.

89. Giuliano, P. (2003) DNA damage induced by polyglutamine-expanded proteins. *Hum. Mol. Genet.*, **12**, 2301–2309.

90. Bertoni, A., Giuliano, P., Galgani, M., Rotoli, D., Ulianich, L., Adornetto, A., Santillo, M.R., Porcellini, A. and Avvedimento, V.E. (2011) Early and late events induced by polyQ-expanded proteins: Identification of a common pathogenic property of polyQ-expanded proteins. *J. Biol. Chem.*, **286**, 4727–4741.

91. Rudnicki, D.D., Yang, X.W. and Margolis, R.L. (2014) Movement Disorders Genetics and Models: HDL2 Mouse 2nd ed. LeDoux,M.S. (ed) Elsevier.

92. Orr, H.T. (2011) Are Polyglutamine Diseases Expanding? *Neuron*, **70**, 377–378.

Legends to Figures

Figure 1. Generation of a *Drosophila* HDL2 model.

(**A**) Schematic illustrating the *JPH3* gene and antisense product. The CTG repeat on the sense strand corresponds to a CAG repeat on the antisense strand. This CTG/CAG repeat is expanded in HDL2 patients. We chose to express the full-length isoform of the antisense gene product, which was identified by 5' RACE products in a BAC-HDL2 mouse model (4, 10). The construct was modified to include a CAG repeat length of 15 (named *HDL2-Q15*) or 138 (*HDL2-Q138*). (**B**) DNA and protein sequence of the *HDL2-Q15* construct. *HDL2-Q138* is identical except for the CAG repeat region length. Start sites identified by 5' RACE are indicated in green, the polyQ region is purple, and the stop codon is red. (**C**) Schematics of HDL2 variants used in these experiments. *HDL2-Q15* and *–Q138* sequences were cloned in vectors with no tag or 5' fluorescent tags. For tagged constructs, resulting proteins have N-terminal RFP (illustrated in red) or GFP (illustrated in green) tags. The polyQ region is shown in purple.

Figure 2. Localization of HDL2-Q15, HDL2-Q138, HTT-Q138 and Q127-HA across cell types.

(**A**) In *pickpocket>RFP-HDL2-Q15* larval multi-dendritic peripheral neurons, HDL2-Q15 is diffuse throughout the cytoplasm and nucleus. (**B**) *pickpocket>RFP-HDL2-Q138* leads to the formation of nuclear aggregates. (**C**) Aggregates in *pickpocket>RFP-HTT-Q138* larvae are exclusively localized to the cytoplasm, often found peri-nuclear. (**D**) *pickpocket>Q127-HA* causes nuclear aggregation of the polyQ tract; no Q127 is visible in the cytoplasm. (**E**) Using the *mef2-GAL4* muscle driver, RFP-HDL2-Q15 remains diffuse throughout the cytoplasm and nucleus in *mef2>RFP-HDL2-Q15* larvae. (**F**) *mef2>RFP-HDL2-Q138* larvae have large aggregates in the nuclei, along with smaller aggregates or puncta in the cytoplasm. (**G**)

Aggregates remain strictly cytoplasmic in *mef2>RFP-HTT-Q138* larvae. (**H**) Q127-HA aggregates in the nucleus of *mef2>Q127-HA* larvae. Small puncta are rarely observed in the cytoplasm. (**I**) In *elav>RFP-HDL2-Q15* epithelial cells of the salivary gland, the polyQ protein remains diffuse throughout the cytoplasm and nuclei. (**J**) *elav>RFP-HDL2-Q138* larvae have large perinuclear aggregates in the cytoplasm of salivary gland cells, along with lower levels of the soluble protein in the nucleus. (**K**) RFP-HTT-Q138 aggregates are cytoplasmic in salivary glands of *elav>RFP-HTT-Q138* larvae. (**L**) Q127-HA aggregates in the nuclei of salivary gland cells in *elav>Q127-HA* larvae. PolyQ proteins are shown in red (RFP-HDL2-Q15, RFP-HDL2-Q138, RFP-HTT-Q138, or Q127-HA), nuclei stained dark blue (anti-elav, panels A-D; DAPI, panels E-L), and anti-HRP to label neuronal membranes is shown in cyan. Images A-D are z-stacks, while images E-L are single confocal planes.

Figure 3. HTT-Q138 forms large axonal aggregates and disrupts synapse formation at the NMJ, while HDL2-Q138 does not.

(**A**) RFP-HDL2-Q138 localizes to the nuclei of motor neurons in *elav>RFP-HDL2-Q138* larvae. HDL2-Q138 is often observed as a single large nuclear inclusion with low levels of soluble protein in the same nucleus. (**B**) In *elav>RFP-HTT-Q138* larvae, aggregates are never observed inside nuclei. (**C**) In *elav>Q127-HA* larvae, Q127 forms nuclear inclusions. (**D**) In *elav>RFP-HDL2-Q138* animals, the polyQ protein is observed along axons as puncta or small aggregates. (**E**) *elav>RFP-HTT-Q138* larvae have large axonal aggregates. (**F**) In contrast, *elav>Q127* animals have no detectable Q127 along axons. (**G**) In *elav>RFP-HDL2-Q138* larvae, RFP-HDL2-Q138 is visible in the axon near the NMJ (circled). The protein does not usually localize to synaptic terminals at the NMJ, however, it is occasionally found within a bouton (arrowhead).

(**H**) *elav>RFP-HTT-Q138* larvae have soluble and aggregated RFP-HTT-Q138 at the synapse, and expression of mutant HTT induces formation of excess synaptic boutons (arrowheads). (**I**) No polyQ protein is visible at the synapse in *elav>Q127-HA* larvae. No synaptic overgrowth is detected in these animals. (**J**) NMJ from a control *elav>GFP* larvae. PolyQ proteins are labeled red (RFP-HDL2-Q138, RFP-HTT-Q138, or Q127-HA), anti-elav is shown in dark blue to label neuronal nuclei, and anti-HRP staining for labeling axons and synaptic terminals is cyan. Images A-C are single confocal planes, while images D-J are z-stacks.

Figure 4. Addition of a nuclear import or export tag alters localization and toxicity of HDL2 polyQ proteins.

(**A**) Schematic of GFP-HDL2-Q138^{attP2}, the protein resulting from expression of the unmodified construct in the *attP2* genetic docking site. The GFP label is shown in green and the polyQ stretch in magenta. (**B**) The HDL2 polyQ protein aggregates in the nucleus, but is also visible in the cytoplasm (arrowheads) of muscles in *mef2>GFP-HDL2-Q138^{attP2}* larvae. (**C**) *mef2>GFP-HDL2-Q138^{attP2}* expression causes 3rd instar lethality. (**D**) Schematic of GFP-HDL2-Q138-NLS^{attP2}, the protein resulting from expression of the NLS-tagged construct. (**E**) The cytoplasmic polyQ protein contribution is completely absent in *mef2>GFP-HDL2-Q138-NLS^{attP2}* larvae, and the protein is found exclusively in the nucleus. (**F**) *mef2>GFP-HDL2-Q138-NLS^{attP2}* expression results in lethality during the 2nd instar stage. (**G**) Schematic of GFP-HDL2-Q138-NES^{attP2}, the protein resulting from expression of the NES-tagged construct. (**H**) The nuclear polyQ protein contribution is completely ablated in *mef2>GFP-HDL2-Q138-NES^{attP2}* larvae. (**I**) Nuclear export of the polyQ protein suppresses lethality and *mef2>GFP-HDL2-Q138-NES^{attP2}* animals are adult viable. Images are single confocal planes.

Figure 5. Nuclear localization of HDL2-Q138^{attP2} causes a rough eye degenerative phenotype. (**A**) *GMR>GFP* animals express a soluble GFP under control of the *GMR-GAL4* eye driver and were used as a control for GFP expression. (**B**) *GMR>GFP-HDL2-Q138^{attP2}* eyes appear normal. (**C**) Nuclear localization of the polyQ protein induces a rough eye phenotype in *GMR>GFP-HDL2-Q138-NLS^{attP2}* animals. In addition to pigmentation defects, dark necrotic patches (arrowheads) are visible on the surface of the eye. (**D**) *GMR>GFP-HDL2-Q138-NES^{attP2}* eyes appear normal.

Figure 6. Nuclear localization of HDL2-Q138 accelerates motor dysfunction onset and reduces lifespan, while nuclear export restores motor function and lifespan to control levels. (**A**) *elav>GFP-HDL2-Q138^{attP2}, elav>GFP-HDL2-Q138-NLS^{attP2}* and *elav>GFP-HDL2-Q138-NES^{attP2}* flies were briefly vortexed to knock them to the bottom of the vial, and their climbing ability (climb >2 cm in 30 sec) was compared to control *elav* flies at the indicated age. Nuclear localization flies have dramatically impaired motor function by 1 week. At three weeks, *elav>HDL2-Q138^{attP2}* flies fail to climb. For nuclear export flies, climbing ability remains indistinguishable from controls at all time points measured. For each time point, mean percent of flies climbing $\pm$ SEM are: **1 day:** control, 100% $\pm$ 0; GFP-HDL2-Q138, 98% $\pm$ 2.2; GFP-HDL2-Q138-NLS, 98% $\pm$ 2.2; GFP-HDL2-Q138-NES, 96% $\pm$ 2.9; not significant via ANOVA with Tukey's post hoc test. **1 week:** control, 96% $\pm$ 2.9; GFP-HDL2-Q138, 100% $\pm$ 0; GFP-HDL2-Q138-NLS, 6% $\pm$ 3.1, GFP-HDL2-Q138-NES, 96% $\pm$ 2.7; GFP-HDL2-Q138-NLS climbing ability is significantly impaired compared to all other groups, $p<0.0001$ via ANOVA with Tukey's post-hoc. **3 weeks:** control, 97% $\pm$ 2.9; GFP-HDL2-Q138, 0% $\pm$ 0; GFP-HDL2-

Q138-NES, 98% ± 2.0; GFP-HDL2-Q138 climbing ability is significantly impaired compared to all other groups, $p<0.0001$ via ANOVA with Tukey's post-hoc. **5 weeks:** control, 83.71% ± 6.4; GFP-HDL2-Q138-NES, 87.5% ± 5.4; not significant via Student's t test. (**B**) *elav>GFP-HDL2-Q138*^{attP2}*, elav>GFP-HDL2-Q138-NLS*^{attP2} and *elav>GFP-HDL2-Q138-NES*^{attP2} male flies were reared at 29°C and lifespan recorded. Neuronal expression of GFP-HDL2-Q138^{attP2} significantly reduces lifespan compared to control flies (median survival 28 versus 43 days, $p<0.0001$ via Mantel-Cox test). Nuclear localization significantly reduces lifespan compared to both controls and *elav>GFP-HDL2-Q138*^{attP2} animals (median survival 10 days, $p<0.0001$ via Mantel-Cox test). Nuclear export completely suppresses toxicity, and lifespan is not significantly different between control and *elav>GFP-HDL2-Q138-NES*^{attP2} flies (not significant via Mantel-Cox test).

	Nucleus			Cytoplasm		
	Aggregates (large)	Aggregates (small)	Soluble	Aggregates (large)	Aggregates (small)	Soluble
HDL2-Q138						
Neurons	+++	++	++	-	++	-
Muscle	+++	++	++	-	++	-
Epithelial cells	-	-	+	++	++	+
HTT-Q138						
Neurons	-	-	-	+++	++	++
Muscle	-	-	-	++	+++	+
Epithelial cells	-	-	-	+++	++	++
Q127						
Neurons	++	++	+	-	-	-
Muscle	++	++	++	-	+	-
Epithelial cells	+	+++	++	-	-	+

Table 1. HDL2-Q138 localization is distinct from either HTT-Q138 or a pure polyQ tract in *Drosophila*.

HTT-Q138 remains strictly cytoplasmic in *Drosophila*. Q127 alone does not localize to the cytoplasm in epithelial cells or neurons. Q127 is occasionally observed in the cytoplasm of muscle tissue, but only visible as small puncta. In contrast, HDL2-Q138 forms large nuclear inclusions in all cell types tested, except salivary gland epithelial cells, and also forms small aggregates or puncta in cytoplasm.

Abbreviations

ANOVA, analysis of variance; DRPLA, dentatorubro-pallidoluysian atrophy; FTDALS1, frontotemporal dementia and/or amyotrophic lateral sclerosis 1; HD, Huntington disease; HTT, *huntingtin*; HDL2, Huntington disease-like 2; HRP, horseradish peroxidase; JPH3, *junctophilin 3;* MJD, Machado-Joseph disease; DM1, mytotonic dystrophy 1; NMJ, neuromuscular junction; Q, glutamine; SEM, standard error of the mean; sca1, spinocerebellar ataxia 1; SCA2, spinocerebellar ataxia 2; SCA8, spinocerebellar ataxia 8; VNC, ventral nerve cord.

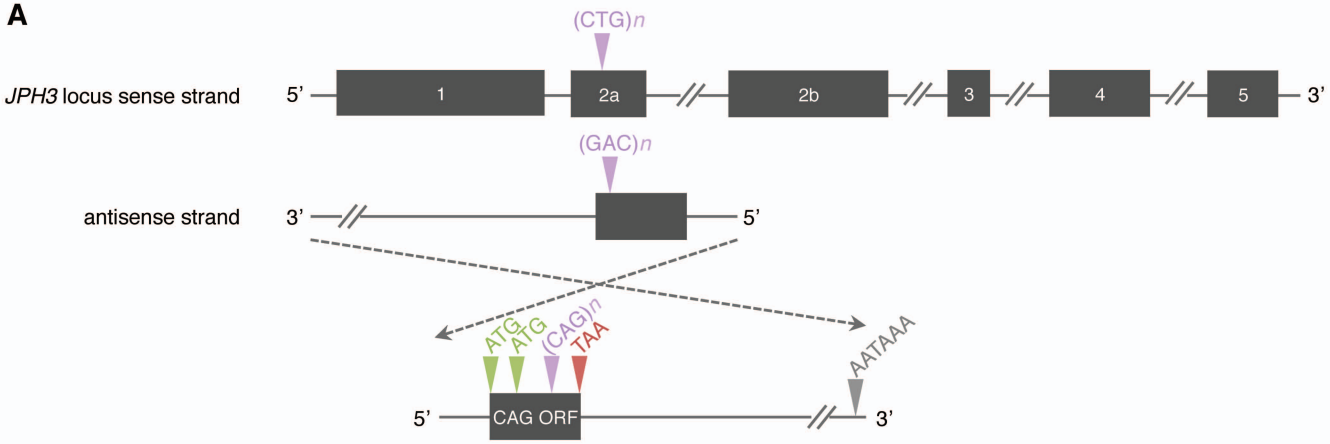

B

```
  1 M  G  V  D  W  S  G  K  P  V  C  L  G  S  G  F  Q  E  R  T
  1 ATGGGAGTGGACTGGTCGGGGAAGCCAGTTTGTTTGGGGTCTGGCTTCCAGGAAAGGACC
 21 G  S  M  R  V  R  C  T  E  E  W  I  S  E  S  P  G  R  R  A
 61 GGCTCCATGCGTGTCAGGTGCACTGAGGAGTGGATATCGGAGAGTCCAGGCAGGCGGGCA
 41 A  A  E  P  A  K  V  P  C  T  E  T  I  L  Q  Q  Q  Q  Q  Q
121 GCTGCAGAGCCGGCCAAGGTTCCCTGCACAGAAACCATCTTACAGCAGCAGCAGCAGCAG
 61 Q  Q  Q  Q  Q  Q  Q  Q  Q  Q  A  A  P  W  L  P  A  P  A  L  P
181 CAGCAGCAGCAGCAGCAGCAGCAGCAGGCAGCTCCCTGGCTTCCGGCCCCGGCTCTGCCC
 81 R  M  R  W  H  L  R  M  K  A  Q  I  D  S  L  N  -
241 CGAATGCGGTGGCATCTTAGAATGAAGGCACAGATCGATTCCCTCAACTAA
```

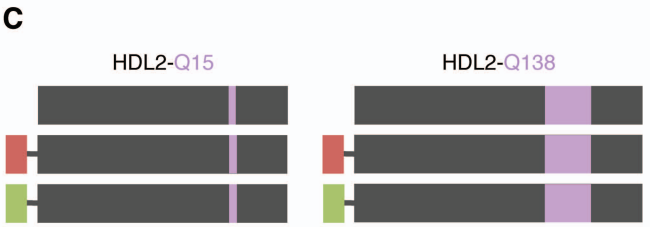

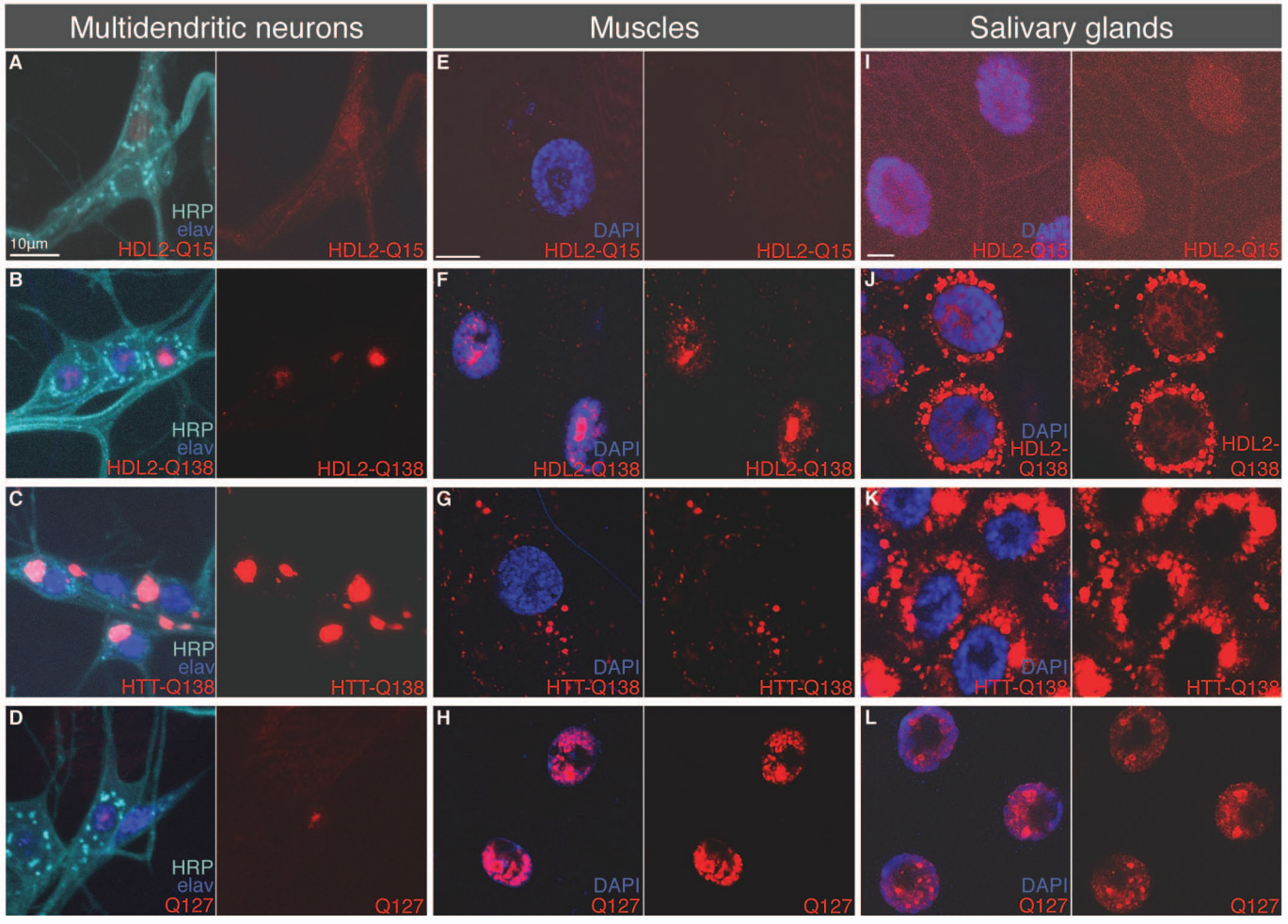
Multidendritic neurons
Muscles
Salivary glands
A
HRP
elav
HDL2-Q15
10µm
HDL2-Q15
E
DAPI
HDL2-Q15
HDL2-Q15
I
DAPI
HDL2-Q15
HDL2-Q15
B
HRP
elav
HDL2-Q138
HDL2-Q138
F
DAPI
HDL2-Q138
HDL2-Q138
J
DAPI
HDL2-
Q138
HDL2-
Q138
C
HRP
elav
HTT-Q138
HTT-Q138
G
DAPI
HTT-Q138
HTT-Q138
K
DAPI
HTT-Q13
HTT-Q13
D
HRP
elav
Q127
Q127
H
DAPI
Q127
Q127
L
DAPI
Q127
Q127

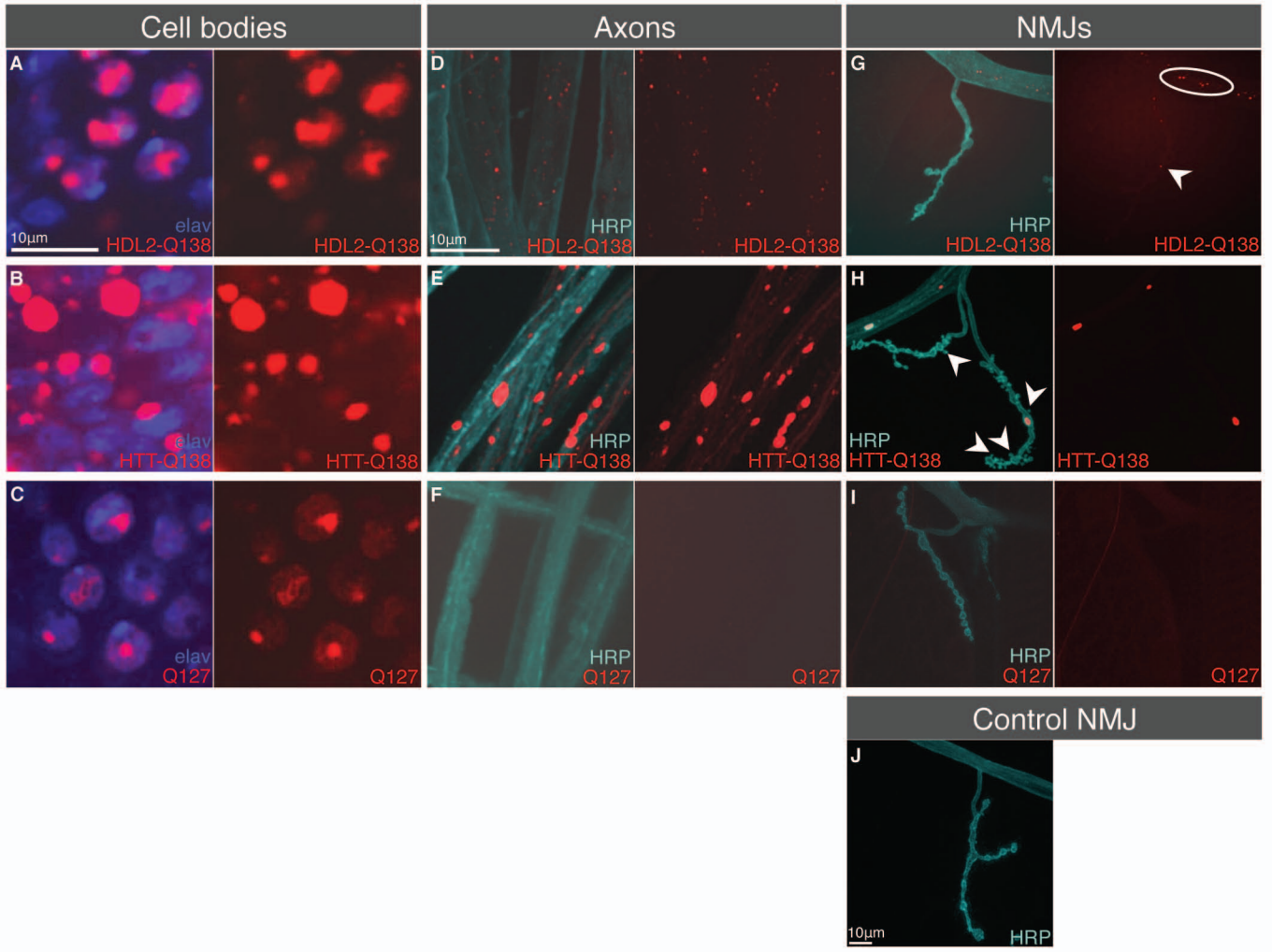
Cell bodies
Axons
NMJs
A
elav
HDL2-Q138
10µm
HDL2-Q138
D
HRP
HDL2-Q138
10µm
HDL2-Q138
G
HRP
HDL2-Q138
HDL2-Q138
B
elav
HTT-Q138
HTT-Q138
E
HRP
HTT-Q138
HTT-Q138
H
HRP
HTT-Q138
HTT-Q138
C
elav
Q127
Q127
F
HRP
Q127
Q127
I
HRP
Q127
Q127
Control NMJ
J
10µm
HRP

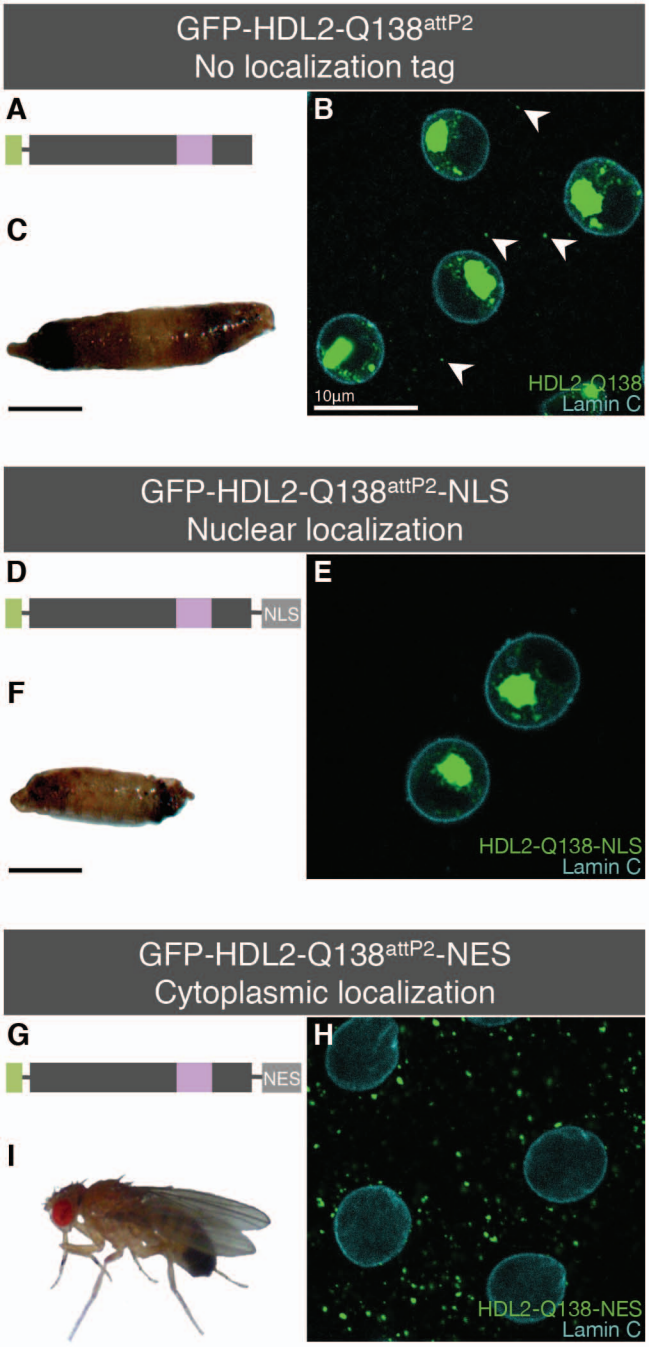
GFP-HDL2-Q138attP2
No localization tag
A
B
C
10µm
HDL2-Q138
Lamin C
GFP-HDL2-Q138attP2-NLS
Nuclear localization
D
NLS
E
F
HDL2-Q138-NLS
Lamin C
GFP-HDL2-Q138attP2-NES
Cytoplasmic localization
G
NES
H
I
HDL2-Q138-NES
Lamin C

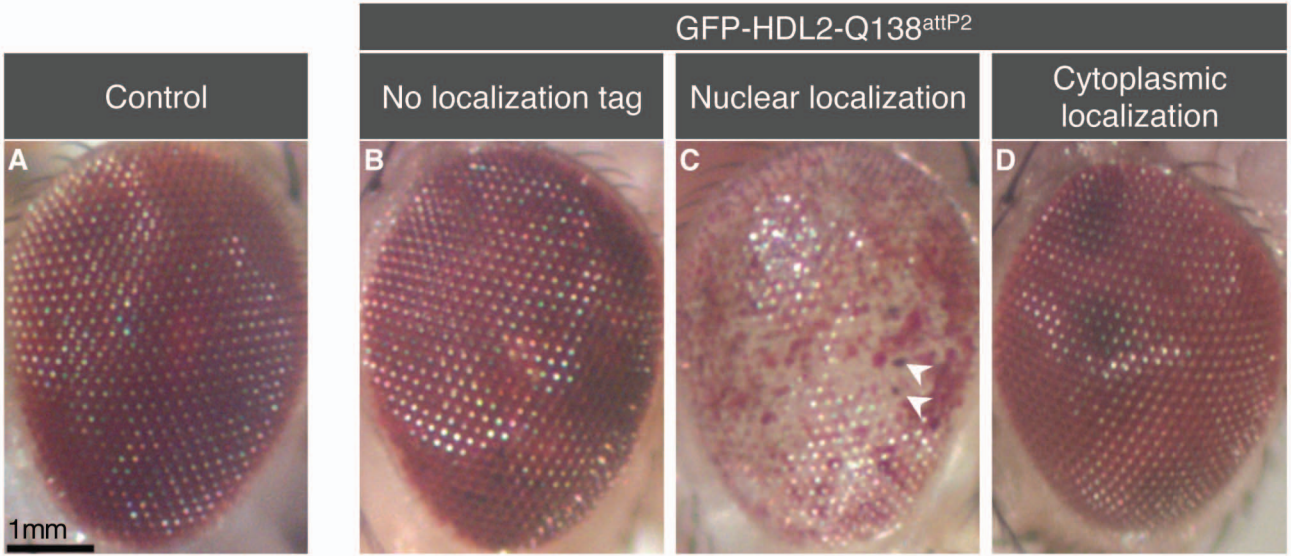
GFP-HDL2-Q138attP2
Control
No localization tag
Nuclear localization
Cytoplasmic localization
A
B
C
D
1mm

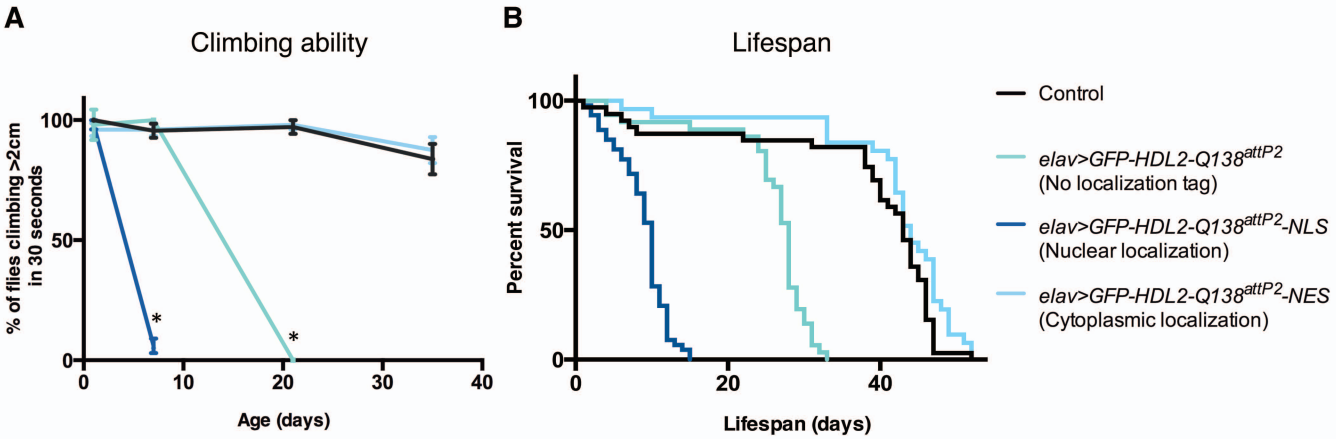

Polyglutamine protein expressed in neurons	Median lifespan (days)	Significant decrease (vs. control)	Significant difference (vs. GFP-HDL2-Q138^{attP2})
Control	43		Yes*
GFP-HDL2-Q138^{attP2} No localization tag	28	Yes*	
GFP-HDL2-Q138^{attP2}-NLS Nuclear localization	10	Yes*	Yes*
GFP-HDL2-Q138^{attP2}-NES Cytoplasmic localization	44	No	Yes*

*p<0.0001